

Palaeodepositional and Hydrocarbon Source-rock characteristics of Sonari succession (Palaeocene), Barmer Basin, NW India: Implications from petrography and geochemistry

Vikram P. Singh^{a*}, Bhagwan D. Singh^a, Runcie P. Mathews^a, Alpna Singh^a, Vinod A. Mendhe^b, Subhashree Mishra^c, Mollika Banerjee^b

^aDST-Birbal Sahni Institute of Palaeosciences, 53-University Road, Lucknow-226 007, India

^bCSIR-Central Institute of Mining and Fuel Research, Barwa Road, Dhanbad-826 015, India

^cCSIR-National Institute of Oceanography, Dona Paula, Goa-403 004, India

*Corresponding author: E-mail address: vikram_chauhan@bsip.res.in (V.P. Singh)

Abstract

Lignite deposits, associated with Akli Formation (Palaeocene), from the Sonari mine of Barmer Basin, Rajasthan, have been investigated by applying organic petrography, palynofacies, and geochemistry in order to understand the origin, nature and character of these lignite-bearing deposits, besides to assess their thermal maturation and hydrocarbon generation potentiality. The studied samples contain an abundance of huminite group of macerals (av. 54.0 vol.%) and relatively higher abundance of C₂₇ and C₂₉ *n*-alkane hydrocarbons. A high carbon preference index (CPI: 5.03-9.44), and terrigenous aquatic ratio (TAR: 5.09-20.01), together with the liptinite macerals (av. 10.3 vol.%), advise the prevailing contribution of higher plants. Besides, the significant amount of detrohuminites (av. 26.8 vol.%) and non-biostructure phytoclasts (av. 42.25%), along with hopanoids denoting a meaningful herbaceous plants input and/or high level of tissue-destruction (bacterial activity). The terpenoid composition is mainly constituted by pentacyclic triterpenoids and A-ring degraded angiosperm derived compounds and diterpenoids. The inertinite contents (av. 22.3 vol.%) and the pristane/phytane (Pr/Ph) ratio imply the variation in the redox conditions during the accumulation. The petrographic indices reveal that the palaeo-flora were accumulated in a limno-telmatic condition, with fluctuating groundwater level. Likewise, the palynofacies data displays that the peat was deposited in dysoxic-suboxic settings under proximal condition. Subsequently, the incidence of dinoflagellate cysts in the studied samples suggest a marine intrusion. The considerable total of pyrite (up to 16.7 vol.%, comprising framboidal) suggests a coastal swamp condition (marginal marine).

The thermal alteration index (TAI: av. 2.15), T_{max} (av. 411 °C for lignite, and 414 °C for associated shale) and the gross calorific values (av. 4601 cal/g) showing the immaturity of the studied sample. The lignites contains low to moderate ash yields (av. 12.57 wt.%) and moisture (av. 12.79 wt.%) contents. Whereas the carbon^{daf} (daf= dry-ash-free basis) contents are high (av. 67.22 wt.%), corroborated well with the inertinite group of macerals. The fuel ratio varies from 0.77 to 1.32. The volatile matter yield^{daf} (av. 51.09 wt.%), fixed carbon^{daf} (av. 48.91 wt.%) and the oxygen^{daf} (av. 22.16 wt.%) contents are moderately high. The total organic carbon contents (TOC: 1.17-54.84 wt.%, av. 24.78 wt.%) and hydrogen index values (HI: 32-361 mg HC/g rock) exhibiting that the studied samples mostly have type III kerogen and show an excellent potentiality to generate gaseous hydrocarbons.

Keywords: Petrography, Palynofacies, Biomarkers, Dinoflagellate cysts, Immature, Gaseous hydrocarbon, Palaeocene deposits

Introduction

The Indian subcontinent, has crossed through different climatic zones, witnessed a rapid growth in the vegetation during its “longest journey” (Morley, 2000). An isolated Indian subcontinent has also experienced many enthralling changes during its voyage to north, as the consequence of the ‘disastrous’ global events of the Palaeogene period, i.e. greenhouse forcing (Sluijs et al. 2005, 2006, 2007), significant transient warming events (Zachos et al. 1993, 2003, 2005), immense discharge of CH₄ hydrates (Svensen et al. 2004), huge alterations in the global carbon phase (Haq et al. 1987; Kennett and Stott, 1991; Dickens et al. 1995) etc. These changes are generally governed by the various geological processes (plate tectonics, volcanic, etc.), and influence the physical, chemical and botanical framework of the region, and later recorded in the sedimentary successions. The formation of these successions during the Palaeocene-Eocene period in the western part of India, in response to the progressive withdrawal of Neotethys, have valuable signatures of palaeoclimatic and palaeoenvironmental changes (Sahni et al. 2006; and references therein). Further, these sequences also hold the economically significant lignite-bearing successions in Kachchh, Saurashtra and Cambay basins of Gujarat state, and, Barmer and Bikaner-Nagaur basins of Rajasthan state.

The north-western Indian state of Rajasthan holds many significant lignite-bearing successions. The excavation of lignite deposits is underway at Kasnau-Matasuk, Palana, Barsingsar, Gurha (Bikaner-Nagaur Basin), Giral, Kapurdi and Sonari (Barmer Basin) mines (Fig. 1a). The lignite-bearing sediments of Akli Formation in Barmer Basin had previously been investigated to understand the past fauna and flora in the region (Tripathi et al. 2003, 2009; Rana et al. 2005, 2006; Singh and Tripathi, 2010; Singh, 2015, etc.). Singh et al. (2016) have discussed the evolution of peat-swamp from the lignite deposits of Giral mine, while Shivanna et al. (2017) presented the fungal-faunal interaction from the Kapurdi mine of the basin. Recently, Prasad et al. (2020) have documented the biostratigraphical framework and sea-level changes during pre-collisional phase of the Indian plate from the Giral lignite section. Kumar et al. (2020) have evaluated the hydrocarbon potential and climatic configuration during the deposition of lignite-bearing sequences in Barmer Basin. Nagori and Khosla (2019) have recovered two new species of early Eocene ostracods (*Stigmatocythere barmerensis* and *S. shivkarensis*) from the Akli Formation of the basin. The Barmer Basin comes under Category-I (productive basin) of the Directorate General of Hydrocarbons, Government of India, and is an essential part of the country's fuel map. The discovery of the Mangala oil field (Block RJ-ON-90-1) in Barmer-Sanchore Basin was one of the most significant onshore oil discoveries in the world during 2001-2010 (Dolson et al. 2015). Since then, the basin has continued in the place of the scientific and industrial communities.

In the studies of coal/lignite-bearing successions, for several decades, the data obtained from organic petrography have undeniably been employed to deduce information about the source vegetation and the conditions under which the peat was accumulated, i.e. the level of groundwater, *Eh* and *pH* of the mire, preservation of plant-tissues, the maturity of the organic matter, its potentiality to generate hydrocarbons, etc. (Taylor et al. 1998, and references therein; Bechtel et al. 2002, 2014; Životić et al. 2010, 2014; Suárez-Ruiz et al. 2012, and references therein; Singh et al. 2010, 2013, 2017 a, b, c; Radhwani et al. 2018; Dai et al. 2020; Mathews et al. 2020). The organic matter characterization based on GC-MS spectroscopy has ever increased in the last few decades for the reconstruction of past depositional environments (Bechtel et al. 2012; Strobl et al. 2014). The chemical architecture of the sediments can efficiently be demonstrated by the biomarker (GC-MS) analysis (Hatcher and Clifford, 1997; Dutta et al. 2009, 2011; Mathews et al. 2018, 2020).

The palynofacies studies, helpful in describing the fine-scale complex changes experienced by the palaeovegetation (peat-forming) during the transportation (towards basin) and after deposition (Tyson, 1995; Batten, 1996a; Mendonça Filho and Gonçalves, 2017). The physical and chemical attributes are valuable in revealing information about geological history and depositional conditions of the lignite/coal sequences (Ward, 2002). Rock-Eval pyrolysis signals are vital and are broadly used to assess the source-rock potential, and to understand the thermal behavior of the sediments (Peters, 1986; Peters and Cassa, 1994; Garcia-Vallés et al. 2000; Skyes and Snowdown, 2002). Organic petrography and palynofacies observations are also instrumental in providing additional reliable information about source-rock evaluation as it has been observed that due to the mineral-matrix interaction (retention of hydrocarbon), the result of Rock-Eval pyrolysis may alter (Grohmann et al. 2018; El Atfy et al. 2019). Thus, the integrated approach of optical and geochemical studies has an analytical effect on the determination of hydrocarbon potential.

Granted, numerous research works have been done in the Barmer Basin for several years, but less information is available about the Sonari lignite deposits. Besides, the sedimentary sequences along the western coastal margin are excellent sites to understand the climatic and environmental variations of the equatorial positioned Indian landmass during Palaeogene (Scotese and Golanka, 1992). Therefore, here, the different proxies (petrographical, palynofacies, and bulk-geochemical) have been effectively integrated to depict the characteristics (origin and nature) of these lignites, the palaeovegetation that thrives in and around the lignite basin, the depositional settings, and the complex changes underwent during the peat formation. We have also combined the data of macerals, visual kerogens and biomarkers with the results of Rock-Eval pyrolysis to obtain more accurate information about the maturity and hydrocarbon generation potential of the Sonari lignite-bearing succession.

GEOLOGICAL SETTINGS

Sonari mine is located in the Barmer district of Rajasthan, covering an area of 1512.50 ha with an existing annual capacity of 1-million-ton lignite. The mine is situated about 30 km from Barmer town between N 25° 57' 09" to E 26° 00' 29" latitudes and N 71° 15' 42" to E 71° 07' 14" longitudes (Fig. 1b), and falls in the 40 N/8, 40 O/5 Survey of India toposheets. Geologically, the mining area is located in the Barmer Basin, which is one of the hydrocarbons producing basins in the western part of the Indian subcontinent. Consequently, the basin is classified under Category-I with proven commercial productivity (Biswas, 2012). The basin is also called Barmer-Sanchore sub-basin (according to DGH, India), which is essentially a northern extension of the Cambay Basin (Dwivedi, 2016). Despite the uplift and tilting during the Miocene, the hydrocarbon-bearing structures are still intact, and until May 2018, 38 oil fields were discovered with 4.2 billion barrels (500 million tons) of proven oil-in-place. According to the latest Cairn India estimates, 7.8 billion barrels (900-1000 million tons) of oil equivalent resources can be exploited from unconventional and tight reservoirs in the Barmer-Sanchore Basin.

The evolution of basin is related to the breakup of Indian craton during Cretaceous-early Palaeocene that resulted in the formation of the Cambay rift (Sisodia and Singh, 2000). The NNW-orienting long, narrow and deep basin is part of a failed continental rift (Bladon et al. 2015; Dolson et al. 2015). The basin has a general dip towards the south, but the giant Mangala field, the first oil-producing field identified in the basin, is located towards the northern part of the basin (Farrimond et al. 2015). The Precambrian rocks of Malani Igneous Complex and pre-rift sedimentation of Palaeozoic and Jurassic forms the floor of the basin (Pareek, 1981). The sedimentary successions from middle Jurassic to lower Eocene ages are encountered in the Barmer-Sanchore Basin (Das Gupta, 1975; Pareek, 1981; Mishra et al. 1993). According to Bladon et al. (2015), the overall deposition in the basin is classified into pre-rift (basement), early syn-rift (Mesozoic deposits), syn-rift (Palaeogene deposits), and post-rift (Quaternary deposits). The hydrocarbon-bearing horizons belong to the Palaeocene Fatehgarh and Barmer Hill Formations (Compton, 2009; Biswas, 2012). During Palaeocene-Eocene, several intervals of lignite deposition occurred in the basin, encountered in the Dharvi Dungar and Akli Formations (Farrimond et al. 2015). The lignites of Akli Formation are encountered in the mine sections of Barmer Basin and assigned an age of Palaeocene-early Eocene (Tripathi et al., 2009). However, recently Prasad et al. (2020) proposed a Danian-Thantian age (Palaeocene) for the Akli Formation in their study from Giral lignite section. Though, Rana et al. (2006) and Singh (2015) have also considered the Palaeocene age for the Akli Formation. While, Compton (2009) and Dolson et al.

(2015) have pointed that the Akli Formation belongs to the Ypresian-Lutetian age. Nevertheless, the determination of age is beyond the scope of the present study. The generalized geology of the Barmer Basin is furnished in Fig. 2.

SAMPLES AND METHODOLOGIES

Samples of lignite and shale (38 in total) were collected using the channel sampling method from the Sonari Lignite Mine. The petrography and bulk-geochemistry were performed on the 17 lignite samples. The palynofacies study has been performed on all the samples. 12 representative samples are utilized for the GC-MS (biomarker) and Rock-Eval pyrolysis analyses, covering all lithologies of the studied succession (Fig. 3).

Petrography

The norms of ISO (ISO-2009) have been followed for the particulate pellets (ISO-7404-2) and maceral analyses (ISO-7404-3). The different groups of macerals (huminite, liptinite, inertinite) were described according to the classification of the International Committee for Coal and Organic Petrology (Sýkorová et al. 2005; Pickel et al. 2017; ICCP, 2001, respectively).

Palynofacies

A minimum of 300-500 counts of the dispersed organic matter (mounted on glass slides) were taken for the palynofacies analysis, after removing the carbonates and silicates with lab grade HCl and HF acids (Batten and Stead, 2005). The dispersed organic matter were classified according to Mendonça Filho and Gonçalves (2017). A Leica DM 3000 microscope has been used for the analysis.

Gas Chromatography-Mass Spectrometry

Briefly, the extraction of the soluble organic matter was carried out by ultrasonication (for 30 minutes), with a mixture of dichloromethane (9): methanol (1). An excess of *n*-hexane (40 ml) used for the precipitation of asphaltenes. An Agilent GC-MS (Agilent 7890A and 5975C) was used for the analyses of separated fraction(s). The instrument conditions are as follows: a fused silica capillary column (HP-5MS) with dimensions 30 m × 0.25 mm i.d., 0.25 μm film thicknesses and the carrier gas (Helium) at 1 ml/min flow rate was used. The temperature in the GC was initially held at 40 °C for 5 min followed

by an increase up to 310 °C at a rate of 4 °C/min and held for 5.5 min. A full scan (m/z 50–550) 70 eV mass spectra were acquired with a source temperature of 300 °C. For data processing, Chemstation software has been used. Assignment of peaks was done using GC retention time, comparison to published mass spectra and MS library.

Proximate and Gross Calorific Value Analyses

The specifications of Bureau of Indian Standard (BIS) and American Society for Testing and Material (ASTM) have been followed for the determination of proximate (BIS-1350, 2003) and the gross calorific values (ASTM D2015, 1996) using muffle furnace and Leco AC 350 GCV analyzer, respectively.

Ultimate Analysis

An Elementar Vario EL III-CHNS analyser was used for the analysis. The norms of the ASTM were followed for the determination of Sulphur (ASTM-D3177-89, 1993a), Carbon and Hydrogen (ASTM-D3178-89, 1993b) and Nitrogen (ASTM-D3179, 1993c).

Rock-Eval Pyrolysis

The pyrolysis analysis was performed in accordance with Espitalié et al. (1985) and Lafargue et al. (1998) using Rock-Eval-6. Based on the lithologies, 10 to 60 mg of powdered samples were progressively heated in the absence of oxygen.

RESULTS

Petrographical Compositions

Table S1 (supplementary 1) shows the frequencies of recorded organic (maceral) and inorganic (mineral matter) portions of the Sonari lignites. The different associations macerals and maceral-mineral matter relations are displayed in Fig. 4.

The huminite group of macerals predominantly prevails, reaching up to 81.2 vol.% with an average of 54.0 vol.% (mineral matter-free: av. 62.1 vol.%) of the total organic matter present in the lignites. The group is characterized principally by the detrohuminite (av. 26.8 vol.%: attrinite +

densinite) and telohuminite (av. 25.7 vol.%: textinite + ulminite) subgroups, while the gelohuminite subgroup has been recorded in a low amount (av. 1.4 vol.%). The most abundant macerals in the samples are ulminite (av. 25.6 vol.%) and densinite (av. 23.4 vol.%). The contents of attrinite are variable, but do not exceed 9.0 vol.%, while textinite (up to 1.8 vol.%) and corpohuminite (av. 1.4 vol.%) macerals have the slightest representations. The inertinite group of macerals has an average of 22.3 vol.% (mmf: av. 26.2 vol.%) of the organic matter. This group has been represented largely by semifusinite (av. 10.4 vol.%), inertodetrinite (av. 6.1 vol.%) and funginite (av. 4.7 vol.%) macerals. The liptinite group of macerals has an average of 10.3 vol.% (mmf: av. 11.8 vol.%) of the total organic matter in the samples. Although, there is no particular pattern of distribution, but, the liptinite contents are slightly higher in the uppermost part of the lignite sequence. Resinite (av. 3.4 vol.%) is the most dominated maceral of this group, followed by sporinite (av. 2.5 vol.%), liptodetrinite (av. 2.2 vol.%), cutinite (av. 2.2 vol.%), and suberinite (av. 0.3 vol.%) macerals.

The mineral matter mostly comprises of pyrite, clay and quartz, besides the sporadic occurrence of siderite and calcite minerals. The minerals are recorded in various forms such as granular, micro-band and as lump form. The contents of the mineral matter range from 4.5 to 26.3 vol.%, with an average of 12.5 vol.%. Pyrite is the most abundant mineral (av. 4.6 vol.%) and recorded mainly in framboidal form along with massive and crystalline forms.

Palynofacies Components

The quantitative distribution of kerogen groups is documented in Table S2 (supplementary 2), and Fig. 5. The components of different kerogen group are shown in Fig. 6.

The studied sediments of Sonari mine manifest the domination of the tissues-derived-phytoclast kerogen group (av. 78.42%), from the terrestrial (mainly) source. The group is further represented by its two subgroups: non-opaque (av. 49.58%) and opaque (av. 28.84%) phytoclasts. In non-opaques, the non-biostructure is the predominant fraction ranging from 3.39 to 65.19% (av. 42.25%), while cuticle (av. 3.55%), biostructure (av. 3.03%), and fungal spores/fruited bodies (av. 0.74%) are in lesser proportions. The opaque OM indicates either aerial oxidation (due to the water column fluctuations and slow subsidence) during the deposition or rework/redeposition (due to the prevalence of corroded types of opaque/black particles) of the OM. The AOM, lacks any botanical identity, is the subdominant group, reaching up to 68.99% (av. 19.26%), principally characterized by the AOM subgroup (av. 19.03%), whereas the resin subgroup (av. 0.15%) appears intermittently. The

palynomorph group is the least in abundance in the studied samples and represented by terrestrial (av. 2.03) and marine (av. 0.29%) components.

Based on the qualitative assessment and relative frequencies of different OM groups, three palynofacies zones have been deduced in the studied succession of Sonari mine (Fig. 5).

Palynofacies zone-I: shows the dominance of phytoclasts (av. 82.32%) with low preservation, as evident by the elevated non-biostructure (NB) contents (av. 43.45%). The opaque phytoclasts (av. 31.15%) are the subdominant fraction of the phytoclasts in this facies. The AOM (av. 15.12%) and palynomorph (av. 2.43%) groups are recorded in fewer proportions. This configuration is marked in the majority of the studied samples (S-1–14, 16–25, 27–32, and S-34–38).

Palynofacies zone-II: has a dominating AOM contents (av. 63.71%) and also a good representation of phytoclasts (av. 33.47%). While the palynomorphs are recorded in low incidence (av. 2.82%). The AOM are mostly terrestrial-derived and are spongy in appearance with no botanical structure. The equidimensional opaque, fungal spore/fruited bodies, and cuticle-cells, along with few dinocysts, are also recorded in lesser proportions. This facies is witnessed only in S-11 and S-26.

Palynofacies zone-III: has a co-dominance of phytoclasts (av. 58.70%) and AOM (av. 41.30%), and marked in S-15 and S-33. The phytoclasts comprised of NB (av. 46.08%), opaques (av. 8.19%), cuticles (av. 2.07%), and fungal remains (av. 1.11%). The AOM are generally terrestrial in origin, however granular AOM has also been observed.

Biomarker Constituents

In the present study, the saturated fractions of lignite and shale extracts have been utilized. Total ion chromatograms and selected ion chromatograms representing (m/z 57), (m/z 191) and (m/z 123) are given in Figs. 7, and 8a and 8b, respectively. The biomarker parameters are presented in Table 1, and the major compounds identified are given in Table 2.

n-Alkanes and Acyclic Isoprenoids

The occurrences of *n*-alkanes and isoprenoids in the studied lignites and shales are recognized based on the mass chromatogram (m/z 57), as showed in Fig. 7. The *n*-alkane distribution generally varies between *n*-C₁₂ and *n*-C₃₃, with peaks maximizing at *n*-C₁₄, *n*- C₁₆, *n*- C₂₇, and *n*- C₂₉. In most samples, the pattern of *n*-alkanes distribution is bimodal. The pristane (Pr) and phytane (Ph) are

recorded and their ratio ranges from 0.71 to 1.35 in shales, while it varies between 1.64 and 3.98 in lignites.

Various *n*-alkane parameters have been calculated that include carbon preference index (CPI), proxy aqueous (P_{aq}), proxy wax (P_{wax}), aliphatic chain length (ACL), and terrigenous aquatic ratio (TAR), and are listed in Table 1. The CPI values range from 2.48 to 4.78 in shales, and from 5.03 to 9.44 in lignites. The values of P_{aq} vary between 0.37 and 0.52 in shales, while in lignites, the values range from 0.10 to 0.35. The P_{wax} values range from 0.60 to 0.74 in shales, and 0.84 to 0.93 in lignites. The ACL varies between 21.19 and 25.65 in shales, whereas in lignites, the values range from 26.89 to 28.23. In shales, the TAR values range from 0.72 to 2.11, while in lignites, the values vary between 5.09 and 20.01. Evidently, a clear distinction in all the parameters is visible in between shale and lignite samples. The shales also showed a lower Pr/*n*-C₁₇ values. However, the Ph/*n*-C₁₈ values are comparable in lignites and shales.

Terpenoids

Plant specific triterpenoid and diterpenoid compounds are present in most of the samples of studied profile with variable abundance. Chiefly, the triterpenoids are in abundance, however, an abundance of diterpenoids has been observed at the basal part. The triterpenoids identified in samples are mainly constituted by pentacyclic triterpenoids and des-A-triterpenoids. Hopanes identified in dominance indicating a high level of bacterial biomass degradation (Fig. 8a). The non-hopanoid pentacyclic triterpenoids identified are the olean-12-ene and urs-2,12-diene. The des-A-triterpenoids compounds include degradation products of oleanane, ursane and lupane (Table 2). The diterpenoids includes isopimarane, *ent*-beyerane, *ent*- α (H)-Kaurane 16 α (H)-phylocladane and *ent*- β (H)-Kaurane (Fig. 8b) are identified.

Bulk-Geochemical Constituents

Proximate, Ultimate and GCV Analyses

Results of the proximate, ultimate and gross calorific value analyses of the Sonari lignite samples are enumerated in Table 3. The lignites have a low to medium moisture content (4.14-19.18%, av. 12.79 wt.%) and ash yields (6.30-23.82%, av. 12.57 wt.%), based on dry-basis (db). The studied lignites are characterized by moderately high fixed carbon contents (dry ash-free (daf): av. 48.91 wt.%) and volatile matter yields (av. 51.09 wt.%, daf). The fuel ratios vary between 0.77 and 1.32. The GCVs

of lignites varies between 3916 and 4945 cal/g (av. 4601 cal/g). The lignites are high in carbon^{daf} (58.26-72.04 wt.%) and moderate in oxygen^{daf} (17.99-31.25 wt.%) contents. The contents of nitrogen^{daf} (2.13-3.27 wt.%) and hydrogen^{daf} (3.56-7.87 wt.%) have been recorded in a lesser amount. The sulphur^{db} contents range from 0.47 to 2.04% (av. 1.26 wt.%) in the lignites. The values of H/C and O/C (atomic ratios) vary between 0.64-1.38 and 0.19-0.40, respectively.

Rock-Eval pyrolysis and Total Organic Carbon Analyses

The measured values and calculated indices are enumerated in Table 4. The free hydrocarbons, marked by the S1 peak of pyrolysis, range from 0.04 to 1.13 mg HC/g (av. 0.40 mg HC/g) for shale, and 0.8 to 2.69 mg HC/g (av. 1.70 mg HC/g rock) for the lignite samples. The remaining hydrocarbons, depicted by S2 peak, generated as a result of breaking of larger molecules of the organic matter range from 0.61 to 56.14 mg HC/g rock (av. 11.4 mg HC/g rock) and 20.5 to 80.62 mg HC/g (av. 52.65 mg HC/g rock) for the shale and lignite samples, respectively. The values of CO₂ generated from the organic matter, as indicated by S3 peak, are 6.04 mg CO₂/g (for shales) and 23.17 mg CO₂/g (for lignites) with an overall average value of 22.55 mg CO₂/g rock. The average values of TOC contents are 8.30 wt.% (in shales) and 41.26 wt.% (in lignites). The average values T_{max}, hydrogen index (HI), and oxygen index (OI) are 414 and 411 °C, 95 and 124 mg HC/g TOC, and 102 and 57.3 mg CO₂/g TOC, respectively for the shale and lignite samples.

DISCUSSION

Peat-Forming Palaeovegetation

The study revealed that the Sonari lignites are chiefly constituted of huminite group of macerals along with the raised contents of inertinites, while liptinites contribute least to the organic composition of the palaeopeat. The elevated value of telohuminites (mainly maceral ulminite) depicts that the higher plants largely contributed to the peat formation. Likewise, the domination of phytoclasts OM, along with the moderate contents (although the liptinite group is low) of macerals resinite, cutinite and sporinite also point towards the terrestrial (higher plants) inputs in the basin. Further, the pentacyclic non-hopanoid compounds with oleanene, ursane and lupane structures are indicative of the angiosperm inputs (Karrer et al. 1977; Sukh Dev, 1989). In the studied samples, the presence of olean-12ene, ursa-2(12)-diene and A-ring degraded compounds suggests that angiosperms were one of the vegetal sources. Recorded palynotaxa from the lignite-bearing Akli Formation belong to the angiosperm

families Arecaceae, Annonaceae, Lamiaceae, Rubiaceae, Liliaceae, Oleaceae, Caesalpiaceae, Onagraceae, Miliaceae, etc. (Tripathi et al. 2003; Singh, 2015).

The detrohuminite contents (mainly maceral densinite), however, on the other hand, indicate either the contribution of the soft-wood plants/vegetation or the enhanced bacterial degradation of the organic matter. Similarly, the variations in the pattern of *n*-alkanes distribution also suggest the vegetation type as C_{27} , and C_{29} *n*-alkanes are dominant in deciduous trees, while grasses tend to have dominant C_{31} (Cranwell et al. 1973). The predominance of *n*- C_{27} and *n*- C_{29} varies in sample nos. S-10 and 22, *n*- C_{27} is slightly elevated, while in sample nos. S-5, 14, and 36, *n*- C_{29} is raising. In terrestrial higher plants, long-chain lipids are characteristic compounds which are originated from the plant waxes (Eglinton and Hamilton, 1967). Lipids with an intermediate molecular weight (*n*- C_{21} to *n*- C_{25}) are characteristic of sphangum and/or aquatic macrophytes (Ficken et al., 2000), whereas short-chain *n*-alkanes (<20) are characteristic of organic matter derived from the algal material or micro-organisms (Cranwell, 1977).

The studied shales are categorized by the prevalence of short-chain *n*-alkanes, while the lignites depicted the abundance of long-chain *n*-alkanes. The higher abundance of long-chain *n*-alkanes in the lignites suggests more inputs from the vascular plants (terrestrial higher plants), which is further supported by the high CPI and TAR values (Bray and Evans, 1961; Bourbonniere and Meyers, 1996). Terrestrial plant sources show a CPI >3, while mature hydrocarbons have values ~1. In the studied samples, the CPI is generally higher than 3 (except in two shale samples- S-2 and S-26), signifying a higher input of terrestrial organic matter. The contribution of microbial-derived organic matter (*n*- C_{16} and *n*- C_{18}) is relatively higher in these shale samples (Fig. 7). Moreover, the lignite samples show relatively higher values of P_{wax} (av. 0.87) than the shales (av. 0.66), indicating more terrestrial (higher plant) influx during the formation of lignites. Although the P_{aq} index represents the input of organic matter from the aquatic sources, it additionally indicates the presence of moisture or precipitation in the depositional area (Duan et al. 2010; Pu et al. 2010). Higher precipitation and humid conditions correspond to an increased P_{aq} value, while decreased precipitation corresponds to relatively drier conditions and low P_{aq} value (Pu et al. 2011). Here in Sonari samples, the P_{aq} values are high in shales, whereas low in lignites (Table 1).

The occurrence of pteridophytic spores in palynological assemblages of the lignite-bearing Akli Formation suggests the contribution from ferns (Tripathi et al. 2003; Singh, 2015). Generally, hopanes are considered to be derived from the cell membranes of prokaryotic organisms (Ourisson and Albrecht, 1992; Sinninghe Damsté et al. 1995). However, ferns can also be a source of hopanes with carbon atoms less than 30 (Đoković et al. 2015). Therefore, to an extent, hopanes in the studied samples

(<30 carbon atoms) can probably be attributed to ferns also, belonging to the families Cyatheaceae, Lycopodiaceae, Osmundaceae, Polypodiaceae, etc. of tropical to subtropical forests (Tripathi et al. 2003).

The presence of diterpenoids with kauranes and phyllocladane skeleton are indicative of the gymnosperm (conifer) sources (Stefanova, 2004; Đoković et al. 2015). These compounds have been found in bottom lignite seam sample (S-36) where it is dominant and also in other samples, where it co-occurs with angiosperm markers. Earlier studies also recoded isolated occurrences of conifers in the Palaeogene sediments of Western India (Paul and Dutta, 2016; Mathews et al. 2020; Chetia et al., 2022). The variations in the relative abundance of terpenoid compounds indicate temporal change in the floral composition in the basin.

Depositional Palaeoenvironment

The maceral compositions and the various maceral-derived indices are significantly helpful in interpreting the palaeodepositional settings of the peat-forming vegetal matter (Diessel, 1992; Silva et al. 2008; Singh et al. 2013, 2017 a; Methews et al. 2020). Nevertheless, few workers were also argued against these indices (Crosdale, 1993; Wüst et al. 2001; Scott, 2002; Moore and Shearer, 2003). Hence, here we are using these petrographic facies models consciously, along with generated palynofacies and organic geochemical data, and available palynological information. In 1986, Diessel proposed an x-y diagram model based on gelification index (GI) and tissue preservation index (TPI), to understand the depositional settings of the Permian coals. Later, these indices (GI and TPI) have been re-estimated for the Palaeogene-Neogene (Cenozoic) coal/lignites by several workers (Kalkreuth et al. 1991; Kalaitzidis et al. 2001, 2004; Flores, 2002; Mavridou et al. 2003). Here, Kalaitzidis et al. (2004) formulae are used as:

$$\text{Gelification Index} = \frac{(\text{ulminite} + \text{gelohuminite} + \text{densinite})}{(\text{textinite} + \text{attrinite} + \text{inertinite})}$$

$$\text{Tissue Preservation Index} = \frac{(\text{telohuminite} + \text{corpohuminite} + \text{fusinite})}{(\text{attrinite} + \text{densinite} + \text{gelinite} + \text{inertodetrinite})}$$

The studied Sonari lignites have a high GI value (0.87-8.69, av. 2.83) and low to moderate TPI values (0.29-1.73 except for one value 3.51, av. 0.94; Table S1). The extrapolation of these values suggesting that the limno-telmatic peat-forming flora was accumulated in the coastal (back-barrier)

setting (Fig. 9). Lower TPI values (<1) agreed on the appearance of herbaceous vegetation, while higher values (>1) indicate the presence of higher plants. This evaluation is also reinforced by the maceral compositions (co-dominance of telohuminite and detrohuminite; Table S1).

Another facies model has been put forward by Calder et al. (1991) to know the relationship between groundwater/hydrological conditions (groundwater index: GWI), and the vegetal input (vegetation index: VI) in the palaeomire. In the present study, the GWI and VI formulae given in Kalaitzidis et al. (2004), together with the minor improvement as advised by Stock et al. (2016) in GWI are used as follows:

$$\text{Ground Water Index} = \frac{(\text{corpohuminite} + \text{gelinite} + \text{densinite} + (\text{Ash}/2))}{(\text{textinite} + \text{ulminite} + \text{attrinite})}$$

Vegetation Index

$$= \frac{(\text{telohuminite} + \text{cutinite} + \text{sporinite} + \text{suberinite} + \text{resinite} + \text{semifusinite} + \text{fusinite})}{(\text{detrohuminite} + \text{inertodetrinite} + \text{alginite} + \text{bituminite} + \text{liptodetrinite})}$$

The values of these indices (GWI and VI) vary between 0.40 and 2.23, and from 0.81 to 3.47 (Table S1), respectively, submitting that the peat-precursor was deposited under high groundwater (i.e., mesotrophic to rheotrophic) level (Fig. 10) with fluctuations in hydrological conditions. Apart from the one high value (3.47 in sample S-24), the VI values are uniform, signifying that no major variation in the botanical contribution appears throughout the formation of Sonari lignite. The contents of inertinite are generally enhanced during the oxic condition/prolong aerial exposure or forest fire (fusinite and semifusinite; Scott and Jones, 1994) events. Here in the samples, the significant variations in the frequencies of inertinite group (5.0-39.2 vol.%), represented by semifusinite, inertodetrinite and funginite macerals, also point towards the fluctuating environmental conditions. The low frequency of maceral fusinite (av. 0.9 vol.%), however, excludes the possibility of a wildfire as other macerals (of inertinite group) are relatively higher in concentration.

The pteridophytic spores characterized by taxa associated with families Osmundaceae and Polypodiaceae jointly denote the existence of humid and dense habitat with persistent water in the area (Ramanujam, 1995). The diversity of *Nypa*-like (Arecaceae) pollen in Akli Formation specified the presence of mangrove flora (lagoonal swamp; Tripathi et al. 2009). The marine incursions can be evident with moderate to a high incidence of pyrites (mainly framboidal, Table S1) in the lignites, and corroborated well with the varying ash yields (Table 3). Similarly, the occurrence of gypsum

(CaSO₄·2H₂O) in upper portion of the succession (Fig. 3) indicates more arid and oxic conditions and might be formed from the percolated marine water (Karagiyit et al. 2021 and reference therein). The presence of dinoflagellate cysts (including the warm water *Apectodinium*; Tripathi et al. 2003) at different levels also suggests the marine incursions in the lignite-bearing sedimentary succession of the Sonari mine.

Since environmental conditions play a vital role in the floral composition, which is having different *n*-alkanes chain length, odd-even preference (OEP), etc. The variation in average chain length (ACL₂₇₋₃₃) reflects the variation in the vegetation inputs (Poynter, 1989). Thus, ACL is considered as an indicator of temperature variation in the source area. The surface temperature of the leaf is directly related to the mean daily maximum temperature. Longer average chains increase the melting point, thus protecting the leaf from elevated temperatures (Rommerskirchen et al. 2003). The plants in colder climates are found to have low ACL as compared to the plants in hotter climates (Eglinton and Hamilton, 1967; Gagosian et al. 1987; Castaneda et al. 2009). However, it should also be noted that the variation of the ACL is distinct to different groups of plants (Hoffmann et al. 2013). The higher ACL values (>29) are generally associated with warm and arid climatic conditions (Sarkar, 2014). In Sonari samples, the ACL vary between 27.66 and 28.71 (Table 1). Therefore, it can be assumed that moderately warm and humid conditions were experienced in the depositional area throughout the lignite formation.

Moreover, the plotting on Tyson's APP diagram shown that the deposition of the majority of samples (34 out of 38) is limited to marginal dysoxic-anoxic basin (II) field. However, the dispersal of samples has also been recorded (two samples in each) in the suboxic-anoxic shelf (VI) and distal-suboxic-anoxic basin (IX) fields (Fig. 11). These fields are also agreeing to the data retrieved from the palynofacies analysis. The marginal dysoxic-anoxic basin (II) or palynofacies zone-I (of the study) has been categorized by the presence of elevated content of phytoclasts, low frequency of AOM, and a minuscule contribution of palynomorphs (Table S2, Fig. 5). Among phytoclasts, the dominant contribution has been made by the non-biostructure components, suggesting that organic matter was altered during and/or after the deposition (Tyson, 1995; Carvalho et al. 2006; Mendonça Filho et al. 2011, 2012; Singh et al., 2021). Further, the overall low values (av. 2.23, Table S2) of PPI (phytoclast preservation index, introduced by Mendonça Filho et al. 2010) specify that the deposition was taken place in proximal (to land) settings. The low frequencies of biostructures, cuticles, and high concentrations of non-biostructures elements of OM in proximal settings might suggest that the influx of oxygenated water (probably marine) in the mire. This in turn, reduces acidity (*pH*) and alters the redox (*Eh*) state of the mire and thus enhanced the bacterial activity that caused the degradation of OM

(Zhang et al. 2010), resulting in the high incidence of non-biostructure elements. Prasad et al. (2020) have also suggested that the accumulation of lignite-bearing deposits in the Giral lignite mine (Akli Formation, Barmer Basin) occurred during highstand systems tract (HST).

Additionally, the relative abundance of pentacyclic triterpenoids (Table 2) also advocates that the destruction of the tissues of peat-vegetation was due to advanced bacterial activity, rather than the mechanical break-down. However, the occurrence of soft-wood flora is also quite evident, which tends to decompose quickly. Further, the high variability in ash yields and an inorganic fraction (mineral matter) also points to the intense degradation of OM that would result in a high accumulation of mineral elements (Davis et al. 2007; Singh et al. 2017b). The low to moderate sulphur contents (Table 3) are generally related to brackish environments (Sachsenhofer et al. 2003) also indicates the proximity of the deposit site to the marine source (Singh et al. 2017b). Accordingly, the moderately high opaque phytoclasts and the inertinite macerals also show the fluctuations in the hydrological condition (mesotrophic-rehotrophic) and/or the probable reworking/redeposition of OM. Besides, the presence of dinoflagellates shows not only the coalescing of terrestrial and marine biota (Fig. 6l), but also a relatively high saline condition. A near shore to the lagoonal depositional environments has also been suggested by Nagori and Khosla (2019), based on the recovery of early Eocene Ostrocods from the lignite-bearing Akli Formation.

The remaining four samples which fall in the suboxic-anoxic shelf (palynofacies zone-II; samples S-11, S-26) and distal-suboxic-anoxic basin (palynofacies zone- III, samples S-15, S-33) fields differ from the palynofacies zone-I with having the high AOM contents, generally associated with the anoxic condition or can be very high in normal marine environment (Mansour et al., 2020b). The anoxic condition in proximal setting was formed as a result of the elevated water column that eventually creates an oxygen-deficient zone, which is ideal for AOM elements (Pacton et al. 2011, Singh et al. 2017 a, b, c; Mansour et al., 2020a; Mathews et al. 2020). This implies that although the depositional condition was more or less similar throughout the studied succession, as is evident, conditions were also changed for a brief period.

Moreover, the Pr/Ph ratio is a widely accepted parameter indicating the redox conditions (Didyk et al. 1978; Hall and Douglas, 1983; Imbus and McKirdy, 1993). However, it should also be noted that the variations in the source of OM (Goossens et al. 1984; Volkman and Maxwell, 1986; ten Haven et al. 1987) and maturity (Tissot and Welte, 1984) affect the Pr/Ph ratio to a great extent. Earlier studies show that Pr/Ph ratio below 0.8 suggests anaerobic conditions, while values between 0.8 and 3 suggest dys-aerobic conditions (Peters et al. 2005). Overall, the Pr/Ph ratio is >1 , suggesting suboxic-oxic condition mostly prevailed in the basin, however two shale samples exhibit little higher values

indicating the variation in the depositional condition. The plotting of Pr/n-C₁₇ vs. Ph/n-C₁₈ (Fig. 12) specifies that these sediments were laid down in a terrestrial-transitional basin setting, and mostly in relatively suboxic-oxic conditions.

Hydrocarbon Generation Potential

The quantity of OM is typically articulated as the total organic carbon (TOC) content, although OM also contains other elements like oxygen, hydrogen, sulphur and nitrogen. In the studied samples, the TOC contents (31.59-45.35 wt.% in lignites, 1.17-17.97 wt.% in shales; Table 4), advocating a good to excellent hydrocarbon potential. The high production and preservation of the OM are usually associated with anoxic conditions (Hunt, 1996). It is also worth noting that the TOC contents are influenced by the inert carbon contents, formed due to the oxidation, high maturity and/or the repositioning of sedimentary matter, and have no potential. Katz (1983) has observed that the oxygen index values are higher for the samples containing a high concentration of carbonate minerals, and decreases with the increase in TOC contents (Ndip et al., 2019). This contention has also been observed in Sonari lignites, the lowest OI value (39 mg CO₂/g TOC) is noted in sample S-36 with highest TOC content (54.84 wt.%), and the highest OI value (76 mg CO₂/g TOC) is recorded in sample S-22 with lowest TOC content (31.59 wt.%). In the shale samples, although highest OI value (187 mg CO₂/g TOC) is observed in the sample S-26 with lowest TOC content (1.17 wt.%), however the reverse is not so obvious. Nevertheless, sample S-15 has the lowest OI value (37 mg CO₂/g TOC) and higher TOC content (15.57 wt.%, very close to highest TOC value (17.97 wt.%) in shales. Thus, it is evident that the inorganic fraction does play an influential role in the quantity of kerogens. Hence, other indicators should also be considered while describing the source potential of the OM (Espitalie et al., 1985; Rullkötter et al., 1988; Peters and Cassa, 1994; Hunt, 1996). The hydrogen index values indicate the quality of OM present in the sediments. It has been observed that the sediments having HI values between 50 and 200 mg HC/g TOC are indicative of type III kerogen (Bordenave and Durand, 1993; Koeverden et al. 2011; Hakimi et al. 2013). In the studied samples, the HI values are below 200 mg HC/g TOC; indicates that these sediments have type III kerogen and can generate gaseous hydrocarbons. As stated earlier, due to the mineral-matrix interaction some of the hydrocarbons can be retained back and may result in low HI values (Grohmann et al. 2018; El Atfy et al. 2019 and references therein).

The cross plots *viz.*, HI vs. TOC (Fig. 13a) and HI vs. OI (Fig. 13b) specify that the OM are mainly contained type III kerogen, and have a gaseous hydrocarbon potentiality. Likewise, the quality

of the source rock can also be articulated by the S2/S3 ratio. The S2/S3 ratio values for the studied samples are <1 (Table 4), indicating the low potential to generate hydrocarbons (Peters and Cassa, 1994). Moreover, S2 signals (threshold value: S2 >4.0 mg HC/g) provide more useful information for assessing the hydrocarbon potential of sediments (Bordenave, 1993; Mendhe et al. 2017a, b). The S2 values recorded for studied samples (shale: av. 11.43 mg HC/g, lignite: av. 52.85 mg HC/g) thus indicates that these sediments have very good hydrocarbon generation potential. The S2 vs. TOC plot also supports the above assessment (Fig. 13c). On the other hand, it was also noted that sediments with good TOC and S2 values do not always produce adequate hydrocarbons because their organic matter is not sufficiently 'cooked'. Therefore, in the process of evaluating the source rock, thermal maturation of the sediments also plays a vital role.

The T_{max} and PI (production index) parameters are used here for the assessment of thermal maturity. In the samples, the T_{max} values are below 435 °C (Table 4), and the plotting of HI vs. T_{max} (Fig. 13d) is indicating the immaturity of these sediments. Similarly, the PI value shows that the samples are well below the zone of oil generation (0.1-0.4%; Hunt, 1996), suggesting the immature nature. The low thermal heating can also result in the high OI values, as the stable oxygen moieties may not break-down (Kotarba et al. 2002; Varma et al. 2015, 2018). The high OI values of the samples also exhibit low thermal maturation. Further, based on the volatile matter yield, carbon content and gross calorific values, these sediments are classed as 'Welch-BraunKohle' and 'lignite' according to the German (DIN) and American (ASTMD-388, 2012) norms, respectively, that also indicates the immaturity of these deposits. Alternatively, thermal alteration index, a 1–5 scale as proposed by Staplin (1969, 1977) based on the colour of sporomorphs (light yellow to yellow-orange then brown and black), has also been used to assess the thermal maturation level *vis-à-vis* hydrocarbon generation potential. The TAI values of the studied samples ranged from 2.00 to 2.50 (with higher values in samples S-13, 36 and 38) advising the immaturity of the OM and potential to generate gaseous (mainly) hydrocarbon (Table S2; Fig. 6).

Furthermore, the plotting of H/C and O/C (Fig. 14) indicates the diagenesis stage of coalification (and hence immature), and the OM constituted of type III (mainly) kerogen. During diagenesis, dehydration causes the formation of monoene counterparts from regular diene pentacyclic nonhopanoid compounds (ten Haven et al. 1992). Therefore, the occurrence of both counterparts also submits that the lignites are immature. Considering hopanes, $\alpha\beta$ configuration is more thermodynamically stable, and is formed during diagenesis (Waples and Machihara, 1991; Vu et al. 2009). In the studied samples, $\alpha\beta$ -homohopane is present. However, the presence of thermally unstable $\beta\beta$ -hopane suggests limited hopanoid alteration, advising thermally immature nature of the OM.

Additionally, the maceral composition (nature and abundance) is also useful in assessing the hydrocarbon generation potentiality (Snowdon, 1991; Taylor et al. 1998). The maceral groups are related to kerogen types, and hence suitable for the verification of source potential. The hydrocarbon generation potentiality of the coal and lignite successions has been the central theme of several studies (Littke et al. 1989; Hunt, 1991; Killips et al. 1994; Wilkins and George, 2002; Sykes et al. 2014). It has been reported in these studies that the heterogeneity of coals/lignites, which is responsible for the variation in hydrocarbon potential, influenced by the maceral constituents, and therefore the conditions under which the peat-forming vegetation was accumulated (Diessel, 1992; Sykes, 2001; Abbassi et al. 2016). The maceral constituents of lignites (huminite > inertinite > liptinite) suggest that the Sonari deposits contained Type III kerogen, and are rich in gaseous hydrocarbon. Further, as a result, the OM recognized in palynofacies analysis mainly contain phytoclasts. The phytoclasts are low in hydrogen content (except cuticle), thus indicate a low (oil/liquid) potentiality (Batten, 1996b). It has also been observed that anoxic conditions are usually associated with good quality of source-rock (Tyson, 1995; Paction et al. 2011; Zhang et al. 2015), favorable for the formation of the AOM. However, the macrophyte-derived AOM (mostly) of Sonari sediments indicates a rather low (oil/liquid) hydrocarbon generation. This data is also well-corroborated with the contents of hydrogen-rich macerals (perhydrous huminite+liptinite: av. 24.5 vol.%), which further supports the low oil potentiality and an excellent gaseous source (with additional heating). This assessment is also consistent with the earlier observations made by Compton (2009), Dolson et al. (2015), and Naidu et al. (2017) that the Barmer Hill and Dharvi Dungar formations are the main source-rocks (lacustrine shales and diatomite) in the Barmer Basin.

Conclusions

An integration of petrography, palynofacies and bulk (and organic) geochemical considerations has been employed for a comprehensive description of nature, composition, palaeovegetation, palaeodepositional settings, potentiality to generate hydrocarbon and, thermal maturity of the Sonari lignite deposits of Barmer Basin. The deductions depicted from the data generated on the Palaeogene deposits of the Akli Formation are complimentary with each other, and also in agreement with the previous researches in Barmer Basin. The prevalence of huminite macerals/phytoclasts OM, higher abundances of long-chain *n*-alkanes, and high values of CPI and TAR are implying that the peat-forming flora was deposited chiefly in anaerobic conditions. The high inertinite contents and the high values of the Pr/Ph ratio, however suggest an intermediate phase of the oxic condition. The palynofloral evidence and the recovery of pentacyclic non-hopanoid compounds with oleanene

structure suggest an angiosperm dominated peat-forming flora. However, the occurrence of diterpenoids and cadalene type of sesquiterpenoid indicate the existence of the gymnosperm sources also.

The studied lignites were formed in limno-telmatic environment with appreciable amount of herbaceous vegetation susceptible to degradation in coastal settings (back-barrier). The variation in the values of GWI-VI indices indicated the shifting (mesotrophic to rheotrophic) in the groundwater levels. The sulphur content in samples is also demonstrating a saline environment (brackish). The values of the PPI and APP diagram indicate that OM accumulates in dysoxic-anoxic condition in proximal (to the source) environments. The occurrence of dinoflagellate cysts is indicative of the inter-mixing of terrestrial and marine elements, also evident by the occurrence framboidal pyrite. The plotting of Pr/n-C₁₇ vs. Ph/n-C₁₈ and Pr/Ph ratio signifying the suboxic conditions prevailed in the basin. The gross calorific values, T_{max}, TAI values, and H/C-O/C plot along with ββ-hopane exhibit the immaturity of these deposits. Although the TOC contents are well-above the threshold values, the lignite deposits of Akli Formation have low to moderate values of HI, PI, and hydrogen-rich macerals, implying that the Sonari sequence has type III kerogen, and capable of generating mainly gaseous hydrocarbons upon maturation.

Acknowledgments

The Director, BSIP (Lucknow) is thanked for permitting the publication of this paper (BSIP/RDCC/23/2021-22). Authors are grateful to the officials of Rajasthan State Mines and Minerals Limited (RSMML, Jaipur) and Sonari Lignite Mine Project (Barmer), Govt. of Rajasthan for their assistance and cooperation during the field work. We acknowledge the help of Dr. Mahesh Shivanna (Ex-BSRA) and Mr. V.P. Singh (Ex-TO) of BSIP during the field visit and laboratory analyses, respectively. We are also thankful to Prof. Suryendu Dutta (Dept. of Earth Science, Indian Institute of Technology Bombay, Mumbai) for extending support for the Rock-Eval pyrolysis and biomarker analyses. VAM and MB are thankful to the Director, CIMFR (Dhanbad) and SM is thankful to the Director, NIO (Goa) for associating with this work. VPS acknowledge SERB, Dept. of Science and Technology (Govt. of India) for granting the National Postdoctoral Fellowship (PDF/2018/000883).

We are also grateful to Dr. John Carranza for his editorial support and to all anonymous reviewers for their constructive suggestions and valuable comments that helped us to improve the earlier version of this article.

References

- Abbassi, S., Edwards, D.S., George, S.C., Volk, H., Mahlstedt, N., di Primio, R., & Horsfield, B. (2016). Petroleum potential and kinetic models for hydrocarbon generation from the Upper Cretaceous to Paleogene Latrobe Group coals and shales in the Gippsland Basin, Australia. *Organic Geochemistry*, 91, 54-67.
- ASTM (American Society for Testing and Material), (1993). Standard Test Method for Sulphur in the Analysis Sample of Coal and Coke, D 3177-89, Annual Book of ASTM standards, Petroleum Products, Lubricants and Fossil Fuels, Vol. 05.05, Gaseous Fuels; Coal and Coke, Philadelphia, PA, pp. 306-309.
- ASTM (American Society for Testing and Material), (1993). Standard Test Method for Carbon and Hydrogen in the Analysis Sample of Coal and Coke, D 3178-89, Annual Book of ASTM standards, Petroleum Products, Lubricants and Fossil Fuels, vol. 05.05, Gaseous Fuels; Coal and Coke, Philadelphia, PA, pp. 310-313.
- ASTM (American Society for Testing and Material), (1993). Standard Test Method for Nitrogen in the Analysis Sample of Coal and Coke, D 3179, Annual Book of ASTM standards, Petroleum Products, Lubricants and Fossil Fuels, vol. 05.05, Gaseous Fuels; Coal and Coke, ASTM, Philadelphia, PA, pp. 314-318.
- ASTM (American Society for Testing and Material), (1996). Standard Test Method for Gross Calorific Value of Solid Fuel by the Adiabatic Bomb Calorimeter, ASTM D2015.
- ASTM (American Society for Testing and Material), Standard Classification of Coals by Rank, ASTM International, West Conshohocken, PA, ASTM D388-12.
- Batten, D.J., (1996a). Palynofacies and palaeoenvironmental interpretation. In: Jansonius, J., Mc Gregor, D.C. (Eds.), *Palynology: Principles and Applications*. AASP 3, 1011-1064.
- Batten, D.J. (1996b). Palynofacies and petroleum potential. In: Jansonius, J., Mc Gregor, D.C. (Eds.), *Palynology: Principles and Applications*. AASP 3, 1065-1084.
- Batten, D.J., & Stead, D.T. (2005). Palynofacies analysis and its stratigraphic application. In: Koutsoukos, E.A.M. (Ed.), *Applied Stratigraphy*. Springer, Dordrecht, Netherlands, pp. 203-226.
- Bechtel, A., Karayiğit, A.I., Sachsenhofer, R.F., İnaner, H., Christanis, K., & Gratzer, R. (2014). Spatial and temporal variability in vegetation and coal facies as reflected by organic petrological and geochemical data in the Middle Miocene Çayirhan coal field (Turkey). *International Journal of Coal Geology*, 134-135, 46–60.
- Bechtel, A., Sachsenhofer, R.F., Kolcon, I., Gratzer, R., Otto, A., & Püttmann, W. (2002). Organic geochemistry of the Lower Miocene Oberdorf lignite (Styrian Basin, Austria): its relation to petrography, palynology and the palaeoenvironment. *International Journal of Coal Geology*, 51, 31–57.
- BIS (Bureau of Indian Standard), (2003). *Methods of Test for Coal and Coke (2nd revision of IS: 1350). Part I, Proximate analysis*. Bureau of Indian Standard, New Delhi, pp. 1-29.

- Biswas, S.K. (2012). Status of Petroleum Exploration in India. Proceedings of Indian National Science Academy, 78, 475-494.
- Bladon, A., Clarke, S.M., & Burley, S.D. (2015). Complex rift geometries resulting from inheritance of pre-existing structures: Insights and regional implications from the Barmer Basin rift. Journal of Structural Geology, 71, 136-154.
- Bordenave, M.L. (1993). Applied Petroleum Geochemistry. Editions Technip, Paris, 524 pp.
- Bordenave, M.L., & Durand, B. (1993). Evolution of ideas and concepts in geochemistry. In: Bordenave, M.L. (Ed.), Applied Petroleum Geochemistry. Editions Technip, pp 5-14.
- Bourbonniere, R.A., & Meyers, P.A. (1996). Sedimentary geolipid records of historical changes in the watersheds and productivities of Lakes Ontario and Erie. Limnology and Oceanography, 41, 352-359.
- Bray, E., & Evans, E. (1961). Distribution of *n*-paraffins as a clue to recognition of source beds. Geochimica et Cosmochimica Acta, 22, 2-15.
- Calder, J.H., Gibbing, M.R., & Mukhopadhyay, P.K. (1991). Peat formation in a Westphalian B piedmont setting, Cumberland Basin, Nova Scotia: implication for the maceral-based interpretation of rheotrophic and raised paleomires. Bulletin de la Société Géologique de France, 162, 283-298.
- Carvalho, M.A., Mendonça Filho, J.G., & Menezes, T.R. (2006). Paleoenvironmental reconstruction based on palynofacies analysis of the Aptian-Albian succession of the Sergipe Basin, North Eastern Brazil. Marine Micropaleontology, 59, 56-81.
- Castañeda, I.S., Werne, J.P., Johnson, T.C., & Filley, T.R. (2009). Late Quaternary vegetation history of southeast Africa: the molecular isotopic record from Lake Malawi. Palaeogeography Palaeoclimatology Palaeoecology, 275, 100-112.
- Chetia, R., Mathews, R.P., Singh, P.K., & Sharma, A. (2022). Conifer-mixed tropical rainforest in the Indian Paleogene: New evidences from terpenoid signatures. Palaeogeography, Palaeoclimatology, Palaeoecology, 596, 110980.
- Compton, P.M. (2009). The geology of the Barmer Basin, Rajasthan, India, and the origins of its major oil reservoir, the Fatehgarh Formation: Petroleum Geoscience, 15, 117–130.
- Cranwell, P.A. (1973). Chain length distribution of *n*-alkanes from lake sediment in relation to post-glacial environmental change. Freshwater Biology, 3, 259–265.
- Cranwell, P.A. (1977). Organic geochemistry of Cam Loch (Sutherland) sediments. Chemical Geology, 20, 205-221.
- Crosdale, P.J. (1993). Coal maceral ratios as indicators of environment of deposition: do they work for ombrogenous mires? Organic Geochemistry, 20, 997-809.
- Dai, S., Bechtel, A., Eble, C.F., Flores, R M., French, D., Graham, I.T., Hood, M.M., Hower, J.C., Korasidis, V.A., Moore, T.A., Püttmann, W., Wei, Q., Zhao, L., & O'Keefe, J.M.K. (2020). Recognition of peat depositional environments in coal: A review. International Journal of Coal Geology, 219, 103383.

- Dai, S., Ren, D., Li, S., Zhao, L., & Zhang, Y. (2007). Coal facies evolution of the main minable coal-bed in the Heidaigou Mine, Jungar Coalfield, Inner Mongolia, northern China. *Science in China Series D Earth Sciences*, 50 (suppl. II), 144-152.
- Das Gupta, S.K. (1975). A revision of the Mesozoic-Tertiary stratigraphy of the Jaisalmer basin, Rajasthan; *Indian Journal of Earth Sciences*, 2, 77-94.
- Davis, R.C., Noon, S.W., & Harrington, J. (2007). The petroleum potential of Tertiary coals from Western Indonesia: relationship to mire type and sequence stratigraphic setting. *International Journal of Coal Geology*, 70, 35-52.
- Dickens, G.R., O'Neil, J.R., Rea, D.K., & Owen, R.M. (1995). Dissociation of oceanic methane hydrate as a cause of the carbon isotope excursion at the end of the Paleocene. *Paleoceanography and Paleoclimatology*, 10(6), 965-971.
- Didyk, B.M., Simoneit, B.R.T., Brassell, S.C., & Eglinton, G. (1978). Organic geochemical indicators of paleoenvironmental conditions of sedimentation. *Nature*, 272, 216-222.
- Diessel, C.F.K. (1986). On the correlation between coal facies and depositional environments. *Proc. 20th Newcastle Symp. The University of Newcastle*, pp. 19-22.
- Diessel, C.F.K. (1992). *Coal-bearing Depositional Systems*. Springer-Verlag, Berlin, 721 pp.
- Doković, N., Mitrović, D., Životić, D., Španić, D., Troškot-Čorbić, T., Cvetković, & O., Stojanović, K. (2015). Preliminary organic geochemical study of lignite from the Smederevsko Pomoravlje field (Kostolac Basin, Serbia) – Reconstruction of geological evolution and potential for rational utilization. *Journal of the Serbian Chemical Society*, 80 (2), 575–588.
- Dolson, J.D., Burley, S.D., Sunder, V.R., Kothari, V., Naidu, B.N., Whiteley, N.P., Farrimond, P., Taylor, A., Direen, N., & Ananthkrishnan B. (2015). The discovery petroleum geology of the Barmer Basin, Rajasthan, India: *American Association of Petroleum Geologists Bulletin*, 99, 433–465.
- Duan, Y., Zheng, C.Y., & Wu, B.X. (2010). Hydrogen isotopic characteristics and their genetic relationships for individual n-alkanes in plants and sediments from Zoigê marsh sedimentary environment. *Science in China Series D Earth Sciences*, 53, 1329-1334.
- Dutta, S., Mallick, M., Bertram, N., Greenwood, P.F., & Mathews, R.P. (2009). Terpenoid composition and class of Tertiary resins from India. *International Journal of Coal Geology*, 80, 44–50.
- Dutta, S., Mathews, R.P., Singh, B.D., Tripathi, S.K.M., Singh, A., Saraswati, P.K., Banerjee, S., & Mann, U. (2011). Petrology, palynology and organic geochemistry of Eocene lignite of Matanomadh, Kutch Basin, western India: implications to depositional environment and hydrocarbon source potential. *International Journal of Coal Geology*, 85, 91-102.
- Dwivedi, A.K. (2016). Petroleum Exploration in India - A perspective and Endeavours. *Proceedings of the Indian National Science Academy* 82 (3), Spl. Issue, pp. 881-903.
- Eglinton, G., & Hamilton, R.J. (1967). Leaf epicuticular waxes. *Science*, 156, 1322-1335.

- El Atfy H., Ghassal, B. I., Maher, A. Hosny, A. Mostafa, A., & Littke, R. (2019). Palynological and organic geochemical studies of the Upper Jurassic-Lower Cretaceous successions, Western Desert, Egypt: Implications for paleoenvironment and hydrocarbon source rock potential. *International Journal of Coal Geology*, 211, 103207.
- Espitalié J., Deroo, G., & Marquis, F. (1985). La pyrolyse Rock-Eval et ses applications (part I). *Revue de l'Institut Français du Pétrole*, 40, 563–579.
- Farrimond, P., Naidu, B.S., Burley, S.D., Dolson, J., Whiteley, N., & Kothari, V. (2015). Geochemical characterization of oils and their source rocks in the Barmer Basin, Rajasthan, India. *Petroleum Geoscience*, 21, 301-321.
- Ficken, K.J., Li, B., Swain, D.L., & Eglinton, G. (2000). An *n*-alkane proxy for the sedimentary input of submerged/floating freshwater aquatic macrophytes. *Organic Geochemistry*, 31, 745-749.
- Ficken, K.J., Wooller, M.J., Swain, D.L., Street-Perrott, F.A., & Eglinton, G. (2002). Reconstruction of a subalpine grass-dominated ecosystem, Lake Rutundu, Mount Kenya: a novel multi-proxy approach. *Paleogeography, Paleoclimatology, Paleoecology*, 177, 137-149.
- Flores, D. (2002). Organic facies and depositional palaeoenvironment of lignites from Rio Major Basin (Portugal). *International Journal of Coal Geology*, 48, 181-195.
- Gagosian, R.B., Peltzer, E.T., & Merrill, J.T. (1987). Long-range transport of terrestrially derived lipids in aerosols from the South-Pacific. *Nature*, 325, 800-804.
- Garcia-Vallés, M., Vendrell-Saz, M., & Pradell-Cara, T. (2000). Organic geochemistry (Rock-Eval) and maturation rank of the Garumnian coal in the Central Pyrenees (Spain). *Fuel*, 79, 505-513.
- Goossens, H., de Leeuw, J.W., Schenck, P.A., & Brassell, S.C. (1984). Tocopherols as likely precursors of pristane in ancient sediments and crude oils. *Nature*, 312, 440–442.
- Grohmann, S., Fietz, S.W., Littke, R., Daher, S.B., Romero-Sarmiento, M.F., Nader, F.H., & Baudin, F. (2018). Source rock characterization of mesozoic to cenozoic organic matter rich marls and shales of the Eratosthenes Seamount, Eastern Mediterranean Sea. *Oil & Gas Science and Technology - Revue d'IFP Energies nouvelles*, 73, 49 (<https://doi.org/10.2516/ogst/2018036>).
- Hakimi, M.H., Abdullah, W.H., Sia, S.G., & Makeen, Y.M. (2013). Organic geochemical and petrographic characteristics of Tertiary coals in the northwest Sarawak, Malaysia: implications for palaeoenvironmental conditions and hydrocarbon generation potential. *Marine Petroleum Geology*, 48, 31-46.
- Hall, P.B., & Douglas, A.G. (1983). The distribution of cyclic alkanes in two lacustrine deposits. In: Bjørøy, M. (Ed.), *Advances in Organic Geochemistry*. John Wiley, Chichester, pp. 576-587.
- Haq, B.U., Hardenbol, J., & Vail, P.R. (1987). Chronology of fluctuating sealevels since the Triassic. *Science*, 235, 1156–1167
- Hatcher, P.G., & Clifford, D.J. (1997). The organic geochemistry of coal: from plant material to coal. *Organic Geochemistry*, 27, 251-274.

- Hoffmann, B., Kahmen, A., Cernusak, L.A., Arndt, S.K., & Sachse, D. (2013). Abundance and distribution of leaf wax n-alkanes in leaves of Acacia and Eucalyptus trees along a strong humidity gradient in northern Australia. *Organic Geochemistry*, 62, 62–67.
- Hunt, J.M., 1991. Generation of gas and oil from coal and other terrestrial organic matter. *Organic Geochemistry*, 17, 673-680.
- Hunt, J.M. (1996). *Petroleum Geochemistry and Geology* (2nd edition). Freeman, New York, 743 pp.
- ICCP, (2001). The new inertinite classification (ICCP System 1994), International Committee for Coal and Organic Petrology. *Fuel*, 80, 459-471.
- Imbus, S.W., & McKirdy, D.M. (1993). Organic geochemistry of Precambrian sedimentary rocks. In: Engel, M.H., Macko, S.A. (Eds.), *Organic Geochemistry*. Plenum Press, New York, pp. 657-684.
- ISO 7404-2, (2009). Methods for the Petrographic Analysis of Bituminous Coal and Anthracite—Part 2: Methods of Preparing Coal Samples. International Organization for Standardization, ISO, Geneva, 8 pp.
- ISO 7404-3, (2009). Methods for the Petrographic Analysis of Bituminous Coal and Anthracite—Part 3: Methods of Determining Maceral Group Composition. International Organization for Standardization, ISO, Geneva, 4 pp.
- ISO 7404-5, (2009). Methods for the Petrographic Analysis of Bituminous Coal and Anthracite—Part 5: Methods of Determining Microscopically the Reflectance of Vitrinite. International Organization for Standardization, ISO, Geneva, 11 pp.
- Kalaitzidis, S., Bouzinos, A., Papazisimou, S., & Christanis, K. (2004). A short-term establishment of forest fen habitat during Pliocene lignite formation in the Ptolemais Basin, NW Macedonia, Greece. *International Journal of Coal Geology*, 57, 243-263.
- Kalaitzidis, S., Papazisimou, S., & Christanis, K. (2001). Forming conditions of the Graikas lignite, Northern Peloponnese. *Bulletin of the Geological Society of Greece XXXIV/3*, 1195 – 1204.
- Kalkreuth, W., Kotis, T., Papanikolaou, C., & Kokkinakis, P. (1991). The geology and coal petrology of a Miocene lignite profile at Meliadi Mine, Katerini, Greece. *International Journal of Coal Geology*, 17, 51-67.
- Karayigit, A.I., Oskay, R.G., & Çelik, Y. (2021). Mineralogy, petrography, and Rock-Eval pyrolysis of late Oligocene coal seams in the Malkara coal field from the Thrace Basin (NW Turkey). *International Journal of Coal Geology*, 244, 103814.
- Karrer, W., Cherbuliez, E., & Eugster, C.H. (1977). *Konstitution und vorkommen der organischen Pflanzenstoffe (exclusive Alkaloide) Ergänzungsband, vol. 1*. Birkhäuser Verlag, Basel.
- Katz, B.J. (1983). Limitations of 'Rock-Eval' pyrolysis for typing organic matter. *Organic Geochemistry*, 4, 195–199.
- Kennett, J.P., & Stott, L.D. (1991). Abrupt deep-sea warming, paleoceanographic changes and benthic extinctions at the end of the Paleocene. *Nature*, 353, 319-322

- Killops, S.D., Woolhouse, A.D., Weston, R.J., & Cook, R.A. (1994). A geochemical appraisal of oil generation in the Taranaki Basin, New Zealand. *American Association of Petroleum Geologists Bulletin*, 78, 1560-1585.
- Koeberden, J.H.V., Karlsen, D.A., & Backer-Owe, K. (2011). Carboniferous non-marine source rocks from Spitsbergen and Bjørnøya: comparison with the western Arctic. *Journal of Petroleum Geology*, 34, 53-66.
- Kotarba, M., Clayton, J., Rice, D., & Wagner, M. (2002). Assessment of hydrocarbon source rock potential of Polish bituminous coals and carbonaceous shales. *Chemical Geology*, 184, 11-35.
- Kumar, A., Singh, A., Paul, D., & Kumar, A. (2020). Evaluation of hydrocarbon potential with insight into climate and environment present during deposition of the Sonari lignite, Barmer Basin Rajasthan. *Energy and Climate Change*, 1, 100006.
- Lafargue, E., Marquis, F., & Pillot, D. (1998). Rock-Eval-6 applications in hydrocarbon exploration, production and soil contamination studies. *Oil Gas Science and Technology*, 53, 421-437.
- Littke, R., Horsfield, B., & Leythaeuser, D. (1989). Hydrocarbon distribution in coals and dispersed organic matter of different maceral compositions and maturities. *Geologische Rundschau*, 78, 391-410.
- Mansour, A., Gentzis, T., Carvajal-Ortiz, H., Tahoun, S.S., Elewa, A.M.T., Mohamed, O., 2020a. Source rock evaluation of the Cenomanian Raha Formation, Bakr oil field, Gulf of Suez, Egypt: Observations from palynofacies, RGB-based sporomorph microscopy, and organic geochemistry. *Journal of Marine and Petroleum Geology*, 122, 104661.
- Mansour, A., Wagreich, M., Gentzis, T., Ocubalidet, S., Tahoun, S.S., Elewa, A.M.T., 2020b. Depositional and organic carbon-controlled regimes during the Coniacian-Santonian event: First results from the southern Tethys (Egypt). *Journal of Marine and Petroleum Geology*, 115, 104285.
- Mathews, R.P., Singh, B.D., & Singh, V.P. (2018). Evaluation of organic matter, hydrocarbon source, and depositional environment of onshore Warkalli sedimentary sequence from Kerala-Konkan Basin, south India. *Journal of the Geological Society of India*, 92(4), 407-418.
- Mathews, R.P., Singh, B.D., Singh, V.P., Singh, A., Singh, H., Shivanna, M., Dutta, S., Mendhe, V.A., & Chetia R. (2020). Organo-petrographic and geochemical characteristics of Gurha lignite deposits, Rajasthan, India: Insights into the palaeovegetation, palaeoenvironment and hydrocarbon source rock potential. *Geoscience Frontiers*, 11, 965-988.
- Mavridou E., Antoniadis P., Khanaqa P., Riegel W., & Gentzis T. 2003. Paleoenvironmental interpretation of the Amynteon-Ptolemaida lignite deposit on northern Greece based on its petrographic composition. *International Journal of Coal Geology*, 56, 253-268.
- Mendhe, V.A., Bannerjee, M., Varma, A.K., Kamble, A.D., Mishra, S., & Singh, B.D. (2017b). Fractal and Pore Dispositions of Coal Seams with Significance to Coalbed Methane Plays of East Bokaro, Jharkhand, India. *Journal of Natural Gas Science and Engineering*, 38, 412-433.
- Mendhe, V.A., Mishra, S., Varma, A.K., Bannerjee, M., Singh, B. D., & Singh, V.P. (2018a). Geochemical and petrophysical characteristics of Permian shale gas reservoirs of Raniganj Basin, West Bengal, India. *International Journal of Coal Geology*, 188, 1-24.

- Mendhe, V.A., Mishra, S., Varma, A.K., Kamble, A.D., Bannerjee, M., & Sutay, T.M. (2017a). Gas Reservoir Characteristics of the Lower Gondwana Shales in Raniganj Basin of Eastern India. *Journal of Petroleum Science and Engineering*, 149, 649–664.
- Mendonça Filho, J.G., & Gonçalves, P.A., (2017). Organic matter: concepts and definitions, Chapter 1. In: Suarez-Ruiz, I., Mendonça Filho, J.G. (Eds.), *Geology: Current and Future Developments. The Role of Organic Petrology in the Exploration of Conventional and Unconventional Hydrocarbon Systems*, 1. Bentham Science Publishers, United Arab Emirates, pp. 1–33.
- Mendonça Filho, J.G., Mendonça, J.O., Menezes, T.R., Oliveira, A.D., Carvalho, M.A., Santanna, A.J., & Souza, J.T. (2010). Palinofácies. In: Carvalho, I.S. (Ed.), *Paleontologia (3rd ed.)* 1, Interciência, Rio de Janeiro, pp. 379-413.
- Mendonça Filho, J.G., Menezes, T.R., & Mendonça, J.O. (2011). Organic composition (palynofacies analysis). Chapter 5, *ICCP Training Course on Dispersed Organic Matter*, pp. 33-81.
- Mendonça Filho, J.G., Menezes, T.R., Mendonça, J.O., Oliveira, A.D., Silva, T.F., Rondon, N.F., & Da Silva, F.S. (2012). Organic Facies: palynofacies and organic geochemistry approaches. In: Panagiotaras, D. (Ed), *Geochemistry– Earth’s System Processes*, InTech, pp. 211-248.
- Mishra, P.C., Singh, N.P., Sharma, D.C., Upadhyay, H., Kakroo, A.K., & Saini, M.L. (1993). Lithostratigraphy of western Rajasthan. Unpublished Oil and Natural Gas Corporation Report, p. 125.
- Moore, T.A., & Shearer, J.C. (2003). Peat/coal type and depositional environment- are they related? *International Journal of Coal Geology*, 56, 233-252.
- Nagori, M.L., & Khosla, S.C. (2019). Early Eocene Ostracoda from the Akli Formation of Barmer Basin, Rajasthan. *Journal of Palaeontological Society of India*, 64(1), 11-26.
- Naidu, B.S., Burley, S.D., Dolson, J., Farrimond, P., Sunder, V.R., Kothari, V., & Mohapatra, P. (2017). Hydrocarbon Generation and Migration Modeling in the Barmer Basin of Western Rajasthan, India: Lessons for Exploration in Rift Basins with Late-Stage Inversion, Uplift and Tilting. In: Abu Ali, M. A., Moretti, I., Nordgård Bolås, H. M. (Eds), *Petroleum Systems Analysis: American Association of Petroleum Geologists Memoir*, 114, 61–94.
- Ndip, E.A., Agyingi, C.M., Nton, M.E., Hower, J.C., & Oladunjoye, M.A. (2019). Organic petrography and petroleum source rock evaluation of the Cretaceous Mamfe Formation, Mamfe basin, southwest Cameroon. *International Journal of Coal Geology*, 202, 27-37.
- Ourisson, G., & Albrecht, P. (1992). Hopanoids. 1. Geohopanoids: the most abundant natural products on Earth? *Accounts of Chemical Research*, 25 (9), 398-402.
- Pacton, M., Gorin, G.E., & Vasconcelos, C. (2011). Amorphous organic matter – experimental data on formation and the role of microbes. *Review of Palaeobotany and Palynology*, 166, 253–267.
- Pareek, H.S. (1981). Basin configuration and sedimentary stratigraphy of western Rajasthan. *Journal of the Geological Society of India*, 22, 517-527.
- Paul, S., & Dutta, S. (2016). Terpenoid composition of fossil resins from western India: New insights into the occurrence of resin-producing trees in Early Paleogene equatorial rainforest of Asia. *International Journal of Coal Geology*, 167, 65-74.

- Peters, K.E. (1986). Guidelines for evaluating petroleum source rock using programmed pyrolysis. *American Association of Petroleum Geologists Bulletin*, 70, 318-386.
- Peters, K.E., & Cassa M.R. (1994). Applied source rock geochemistry. In: Magoon, L.B., Dow, W.G. (Eds.), *The Petroleum System from Source to Trap*, American Association of Petroleum Geologists Memoir, 60, 93-120.
- Peters, K.E., Walters, C.C., & Moldowan, J.M. (2005). *The Biomarker Guide*. Cambridge University, New York, 1132 pp.
- Pickel, W., Kus, J., Flores, D., Kalaitzidis, S., Christanis, K., Cardott, B.J., Misz-Kennan, M., Rodrigues, S., Hentschel, A., Hamor-Vido, M., Crosdale, P., Wagner, N., & ICCP. (2017). Classification of liptinite – ICCP System 1994. *International Journal of Coal Geology*, 169, 40-61.
- Poynter, J. (1989). *Molecular Stratigraphy: The Recognition of Palaeoclimatic Signals in Organic Geochemical Data*. University of Bristol, England.
- Prasad, V., Singh, I.B., Bajpai, S., Garg, R., Thakur, B., Singh, A., Saravanan, N., & Kapur, V.V. (2013). Palynofacies and sedimentology-based high-resolution sequence stratigraphy of the lignite-bearing muddy coastal deposits (early Eocene) in the Vastan Lignite Mine, Gulf of Cambay, India. *Facies*, 59, 737-761.
- Pu, Y., Zhang, H.C., Lei, G.L., Chang, F.Q., Yang, M.S., Zhang, W.X., Lei, Y.B., Yang, L.Q., & Pang, Y.Z. (2010). Climate variability recorded by *n*-alkanes of paleolake sediment in Qaidam Basin on the northeast Tibetan Plateau in late MIS3. *Science China: Earth Sciences*, 53, 863–870
- Pu, Y., Zhang, H.C., Wang, Y.L., Lei, G.L., Nace, T., Zhang, S.P., 2011. Climatic and environmental implications from *n*-alkanes in glacially eroded lake sediments in Tibetan Plateau: An example from Ximen Co. *Chinese Science Bulletin*, 56, 1503–1510.
- Radhwani, M., Bechtel, A., Singh, V.P., Singh, B.D., & Mannai-Tayeche, B. (2018). Petrographic, palynofacies and geochemical characteristics of organic matter in the Saouef Formation (NE Tunisia): Origin, paleoenvironment, and economic significance. *International Journal of Coal Geology*, 187, 114-130.
- Rai, J., Singh, A., & Pandey, D.K. (2013). Early to Middle Albian age calcareous nannofossils from Pariwar Formation of Jaisalmer Basin, Rajasthan, western India and their significance. *Current Science* 105(11), 1604-1611.
- Ramanujam, C.G.K. (1995). Pteridophytes during the Tertiary period of south India as revealed by their characteristic sporomorphs. *The Palaeobotanist*, 44, 152-156.
- Rana, R.S., Kumar, K., Loyal, R.S., Sahni, A., Rose, K. D., Mussell, J., Singh, H., & Kulshreshtha, S.K. (2006). Selachians from the early Eocene Kapurdi Formation (Fuller's Earth), Barmer district, Rajasthan. *Journal of the Geological Society of India*, 67(4), 509-522.
- Rana, R.S., Kumar, K., Singh, H., & Rose, K.D. (2005). Lower vertebrates from the late Palaeocene-earliest Eocene Akli Formation Giral Lignite Mine Barmer District western India. *Current Science*, 89, 1606–1613.

- Rommerskirchen, F., Eglinton, G., & Dupont, L. (2003). A north to south transect of Holocene southeast Atlantic continental margin sediments: relationship between aerosol transport and compound-specific $\delta^{13}\text{C}$ land plant biomarker and pollen records. *Geochemistry, Geophysics, Geosystem*, 4, 1101. doi:10.1029/2003GC000541.
- Rullkötter, J., Peakman, T.M., & ten Haven, H.L. (1994). Early diagenesis of terrigenous triterpenoids and its implications for petroleum geochemistry. *Organic Geochemistry*, 21, 215-233.
- Sachsenhofer, R.F., Bechtel, A., Reischenbacher, D., & Weiss, A. (2003). Evolution of lacustrine systems along the Miocene Mur-Mürz fault system (Eastern Alps, Austria) and implications on source rocks in pull-apart basins. *Marine and Petroleum Geology*, 20, 83-110.
- Sahni, A., Saraswati, P.K., Rana, R.S., Kumar, K., Singh, H., Alimohmmadian, H., Sahni, N., Rose, K.D., Singh, L., & Smith, T. (2006). Temporal constraints and depositional environments of the Vastan lignite sequence, Gujarat: analogy for the Cambay Shale hydrocarbon source rock. *Journal of Petroleum Geology*, 15, 1-20.
- Sarkar, S. (2014). Holocene Variations in the Strength of the Indian Monsoon System: A Combined Biomarker and Stable Isotope Approach. Institut für Erd- und Umweltwissenschaften, Universität Potsdam. Ph.D. thesis, p.114.
- Scotese, C.P., & Golanka, J. (1992). Paleogeographic atlas, PALEOMAP progress report 20-0692. University of Texas, Arlington, 34.
- Scott, A.C. (2002). Coal petrology and the origin of coal macerals: a way ahead? *International Journal of Coal Geology*, 50, 119-134.
- Scott, A.C., & Jones, T.P. (1994). The nature and influence of fire in Carboniferous ecosystems. *Palaeogeography, Palaeoclimatology, Palaeoecology*, 106, 91–112.
- Shivanna, M., Singh, A., Singh, B.D., Singh, V.P., Matthews, R.P., & Souza, P.A. (2017). Peat biomass degradation: Evidence from fungal and faunal activity in carbonized wood from the Eocene sediments of western India. *Palaeoworld*, 26, 531–542.
- Silva, M.B., Kalkreuth, W., & Holz, M. (2008). Coal petrology of coal seams from the Leão-Butiá Coalfield, Lower Permian of the Paraná Basin, Brazil: implications for coal facies interpretations. *International Journal of Coal Geology*, 73, 331-358.
- Singh, A., Mahesh, S., Singh, H., Tripathi, S.K.M., & Singh, B.D. (2013). Characterization of Mangrol lignite (Gujarat), India: Petrography, palynology, and palynofacies. *International Journal of Coal Geology*, 120, 82-94.
- Singh, A., Shivanna, M., Mathews, R.P., Singh, B.D., Singh, H., Singh, V.P., & Dutta, S. (2017a). Paleoenvironment of Eocene lignite bearing succession from Bikaner-Nagaur Basin, western India: Organic petrography, palynology, palynofacies and geochemistry. *International Journal of Coal Geology*, 181, 87-102.
- Singh, H. (2015). Palynofloral investigation of the Akli Formation (Palaeocene) of Giral Lignite Mine, Barmer District, Rajasthan. *Geophytology*, 45(2), 209-214.
- Singh, H., & Tripathi, S. K. M. (2010). Fungal remains from the Early Palaeogene subsurface sediments of Barakha, Barmer District, western Rajasthan, India. *Geophytology*, 39(1-2), 9-15.

- Singh, P.K., Rajak, P.K., Singh, M.P., Singh, V.K., Naik, A.S., & Singh, A.K. (2016). Peat swamps at Giral lignite field of Barmer basin, Rajasthan, Western India: understanding the evolution through petrological modeling. *International Journal of Coal Science and Technology*, 3(2), 148–164.
- Singh, P.K., Singh, M.P., & Singh, A.K. (2010). Petro-chemical characterization and evolution of Vastan lignite, Gujarat, India. *International Journal of Coal Geology*, 82, 1–16.
- Singh, V.P., Singh, B.D., Mathews, R.P., Singh, A., Mendhe, V.A., Singh, P.K., Mishra, S., Dutta, S., Shivanna, M., & Singh, M.P. (2017c). Investigation on the lignite deposits of Surkha mine (Saurashtra Basin, Gujarat), western India: Their depositional history and hydrocarbon generation potential. *International Journal of Coal Geology*, 183, 78-99.
- Singh, V.P., Singh, B.D., Singh, A., Singh, M.P., Mathews, R.P., Dutta, S., Mendhe, V.A., Mahesh, S., & Mishra, S. (2017b). Depositional palaeoenvironment and economic potential of Khadsaliya lignite deposits (Saurashtra Basin), western India: Based on petrographic, palynofacies and geochemical characteristics. *International Journal of Coal Geology*, 171, 223-242.
- Singh, V.P., Singh, B.D., Mathews, R.P., Mendhe, V.A., Agnihotri, P., Mishra, S., Radhwani, M., Dutta, S., Subramanian, K.A., Singh, A., & Singh, H. (2021). Petrographical-geochemical characteristics and floral-faunal compositions of the Valia lignite deposits from Cambay Basin (Gujarat), western India. *International Journal of Coal Geology*, 248, 103866.
- Sinninghe Damsté, J.S., Van Duin, A.C.T., Hollander, D., Kohnen, M.E.L., & De Leeuw, J.W. (1995). Early diagenesis of bacteriohopanepolyol derivatives: formation of fossil homohopanoids. *Geochimica et Cosmochimica. Acta*, 59 (24), 5141-5157.
- Sisodia, M.S., & Singh, U.K. (2000). Depositional environment and hydrocarbon prospects of the Barmer Basin, Rajasthan, India. *Nafta*, 51, 309-326.
- Sluijs, A., Brinkhuis, H., Schouten, S., Bohaty, S. M., John, C.M., Zachos, J. C., Sinninghe Damsté, J. S., Crouch, E. M., & Dickens, G.R. (2007). Environmental precursors to light carbon input at the Paleocene/Eocene boundary. *Nature*, 450, 1218–1221.
- Sluijs, A., Pross, J., & Brinkhuis, H. (2005). From greenhouse to icehouse; organic-walled dinoflagellate cysts as paleoenvironmental indicators in the Paleogene, *Earth-Science Reviews*, 68, 281–315,
- Sluijs, A., Schouten, S., Pagani, M., Woltering, M., Brinkhuis, H., Sinninghe Damsté, J. S., Dickens, G.R., Huber, M., Reichert, G.-J., Stein, R., Matthiessen, J., Lourens, L.J., Pedentchouk, N., Backman, J., Moran, K., & the Expedition 302 Scientists (2006). Subtropical Arctic Ocean temperatures during the Palaeocene/Eocene thermal maximum. *Nature*, 441, 610–613,
- Snowdon, L.R. (1991). Oil from type III organic matter: resinite revisited. *Organic Geochemistry*, 17, 743-747.
- Snowdon, L.R. (1995). Rock-Eval T_{max} suppression: Documentation and amelioration. *American Association of Petroleum Geologists Bulletin*, 79, 1337-1348.
- Staplin, F.L. (1969). Sedimentary organic matter, organic metamorphism, and oil and gas occurrence. *Bulletin of Canadian Petroleum Geology*, 17, 47-66.

- Staplin, F.L. (1977). Interpretation of thermal history from colour of particulate organic matter - a review. *Palynology*, 1, 9-18.
- Stefanova, M. (2004). Molecular indicators for *Taxodium dubium* as coal progenitor of “Chukurovo” lignite, Bulgaria. In: *Proceedings of the 10th International Congress, Bulletin of the Geological Society of Greece*, XXXVI, 342-347.
- Stock, Alexander T., Littke, R., Lücke, A., Zieger, L., & Thielemann, T. (2016). Miocene depositional environment and climate in western Europe: the lignite deposits of the Lower Rhine Basin, Germany. *International Journal of Coal Geology*, 157, 2-18.
- Strobl, S.A.I., Sachsenhofer, R.F., Bechtel, A., & Meng, Q. (2014). Paleoenvironment of the Eocene coal seam in the Fushun basin (NE China): Implications from petrography and geochemistry. *International Journal of Coal Geology*, 134-135, 24-37.
- Suárez-Ruiz, I., Flores, D., Mendonça Filho, J.G., & Hackley, P.C. (2012). Review and update of the applications of organic petrology: Part 1, Geological applications. *International Journal of Coal Geology*, 22, 54-112.
- Sukh Dev, (1989). Terpenoids. In: Rowe, J.W. (Ed.), *Natural Products of Wood Plants 1*. Springer, Berlin, pp. 691-807.
- Svensen, H., Planke, S., Malthes-Sørensen, A., Jamtveit, B., Myklebust, R., Eidem, T.R., & Rey, S.S. (2004). Release of methane from a volcanic basin as a mechanism for initial Eocene global warming. *Nature*, 429, 542–545.
- Sykes, R. (2001). Depositional and rank controls on the petroleum potential of coaly source rocks. In: Hill, K.C., Bernecker, T. (Eds.), *Eastern Australasian Basins Symposium, a Refocused Energy Perspective for the Future*. Petroleum Exploration Society of Australia, Special Publication, 591–601.
- Sykes, R., & Snowdon, L. (2002). Guidelines for assessing the petroleum potential of coaly source rocks using Rock-Eval. *Organic Geochemistry*, 33(12), 1441-1455
- Sykes, R., Volk, H., George, S.C., Ahmed, M., Higgs, K.E., Johansen, P.E., & Snowdon, L.R. (2014). Marine influence helps preserves the oil potential of coaly source rocks: Eocene Mangahewa Formation, Taranaki Basin, New Zealand. *Organic Geochemistry*, 66, 140–163.
- Sýkorová, I., Pickel, W., Christanis, K., Wolf, M., Taylor, G.H., & Flores, D. (2005). Classification of huminite— ICCP System 1994. *International Journal of Coal Geology*, 62, 85-106.
- Taylor, G.H., Teichmüller, M., Davis, A., Diessel, C.F.K., Littke, R., & Robert, P. (1998). *Organic Petrology*. Gebrüder Borntraeger, Berlin, 704 pp.
- ten Haven, H.L., de Leeuw, J.W., Rullcötter, J., & Sinninghe Damsté, J.S. (1987). Restricted utility of the pristane/phytane ratio as a palaeoenvironmental indicator. *Nature*, 330, 641–643.
- ten Haven, H.L., Peakman, T.M., & Rullkotter, J. (1992). Δ^2 -Triterpenes: Early intermediates in the diagenesis of terrigenous triterpenoids. *Geochimica et Cosmochimica Acta*, 56, 1993-2000.
- Tissot, B.P., & Welte, D.H. (1984). *Petroleum Formation and Occurrence*. 2nd Edition, Springer: Berlin-Heidelberg-New York, 669 pp

- Tripathi S.K.M., Kumar, M., & Srivastava, D. (2009). Palynology of Lower Palaeogene (Thanetian-Ypresian) coastal deposits from the Barmer Basin (Akli Formation, Western Rajasthan, India): Palaeoenvironmental and palaeoclimatic implications. *Geologica Acta*, (7)1-2, 147-160.
- Tripathi, S.K.M., Singh, U.K., & Sisodia, M.S. (2003). Palynological investigation and environmental interpretation on Akli Formation (Late Palaeocene) from Barmer Basin, western Rajasthan, India. *The Palaeobotanist*, 52, 87-95.
- Tyson, R.V. (1995). *Sedimentary Organic Matter; Organic Facies and Palynofacies*. Chapman & Hall, London, 615 pp.
- Varma, A.K., Hazra, B., Chinara, I., Mendhe, V.A., & Dayal, A.M. (2015). Assessment of organic richness and hydrocarbon generation potential of Raniganj basin shales, West Bengal, India. *Marine and Petroleum Geology*, 59, 480-490.
- Varma, A.K., Mishra, D.K., Samad, S.K., Prasad, A. K., Panigrahi, D.C., Mendhe, V.A., & Singh, B.D. (2018). Geochemical and Organo-petrographic characterization for hydrocarbon generation from Barakar Formation in Auranga Basin, India. *International Journal of Coal Geology*, 186, 97-114.
- Volkman, J.K., & Maxwell, J.R. (1986). Acyclic isoprenoids as biological markers. In: Johns, R.B. (Ed.), *Biological Markers in the Sedimentary Record*. Elsevier, Amsterdam, pp. 1–46.
- Vu, T.T.A., Zink, K.-G., Mangelsdorf, K., Skyes, R., Wilkes, H., & Horsfield, B. (2009). Changes in bulk properties and molecular compositions within New Zealand Coal Band solvent extracts from early diagenetic to catagenetic maturity levels. *Organic Geochemistry*, 40, 963-977.
- Waples, D.W., & Machihara, T. (1991). Biomarkers for geologists: A practical guide to the application of steranes and triterpanes in petroleum geology. *American Association of Petroleum Geologists Methods in Exploration*, No.9, 19-40.
- Ward, C.R. (2002). Analysis and significance of mineral matter in coal seams. *International Journal of Coal Geology*, 50, 135-168.
- Wilkins, W.T., & George, S.C. (2002). Coal as a source rock for oil: A review. *International Journal of Coal Geology*, 50, 317-361.
- Wüst, R.A.J., Hawke, M.I., & Bustin, R.M. (2001). Comparing maceral ratios from tropical peat lands with assumptions from coal studies: do classic coal petrographic interpretation methods have to be discarded? *International Journal of Coal Geology*, 48, 115-132.
- Zachos, J. C., Röhl, U., Schellenberg, S. A., Sluijs, A., Hodell, D. A., Kelly, D. C., Thomas, E., Nicolo, M., Raffi, I., Lourens, L. J., McCarren, H., & Kroon, D. (2005). Rapid Acidification of the Ocean during the Paleocene-Eocene Thermal Maximum. *Science*, 308, 1611–1615.
- Zachos, J.C., Wara, M. W., Bohaty, S., Delaney, M.L., Petrizzo, M.R., Brill, A., Bralower, T. J., & Premoli Silva, I. (2003). A transient rise in tropical sea surface temperature during the Paleocene-Eocene thermal maximum. *Science*, 302, 1551–1554.
- Zachos, J.C., Lohmann, K.C., Walker, J.C.G., & Wise, S.W. (1993). Abrupt climate change and transient climates during the Palaeogene: a marine perspective. *The Journal of Geology*, 101, 191–213.

- Zhang, M., Ji, L., Wu, Y., & He, C. (2015). Palynofacies and geochemical analysis of the Triassic Yanchang Formation, Ordos Basin: Implications for hydrocarbon generation potential and the paleoenvironment of continental source rocks. *International Journal of Coal Geology*, 152, 159–176.
- Zhang, S., Tang, S., Tang, D., Pan, Z., & Yang, F. (2010). The characteristics of coal reservoir pores and coal facies in Liulin district, Hedong coal field of China. *International Journal of Coal Geology*, 81, 117-127.
- Životić, D., Bechtel, A., Sachsenhofer, R., Gratzer, R., Radić, D., Obradović, M., & Stojanović, K. (2014). Petrological and organic geochemical properties of lignite from the Kolubara and Kostolac basins, Serbia: implication on Grindability Index. *International Journal of Coal Geology*, 131, 344–362.
- Životić, D., Jovančičević, B., Schwarzbauer, J., Cvetković, O., Gržetić, I., Ercegovac, M., Stojanović, K., & Šajnović, A. (2010). The petrographical and organic geochemical composition of coal from the East field, Bogovina Basin (Serbia). *International Journal of Coal Geology*, 81, 227-241.

Table 1. The parameters calculated from the distributions of n-alkanes and isoprenoids.

S. no.	Lithology	CPI	TAR	P _{aq}	P _{wax}	Pr/Ph	Pr/n-C ₁₇	Ph/n-C ₁₈	ACL
S-2	Shale	2.48	1.70	0.46	0.65	0.86	1.06	0.46	28.02
S-5	Shale	4.17	2.05	0.37	0.74	1.20	2.32	0.72	28.06
S-10	Lignite	8.30	10.68	0.20	0.89	3.23	3.25	0.71	27.99
S-14	Lignite	9.44	10.06	0.10	0.93	1.64	3.36	0.90	28.41
S-17	Lignite	7.97	20.01	0.16	0.90	2.12	4.28	0.94	28.10
S-19	Shale	4.78	2.11	0.42	0.72	1.19	1.83	0.74	27.71
S-22	Lignite	6.42	5.09	0.35	0.84	3.98	4.28	0.64	27.66
S-26	Shale	2.18	0.72	0.51	0.60	0.71	0.86	0.78	27.89
S-30	Lignite	5.03	11.76	0.23	0.84	3.49	6.14	0.88	28.58
S-33	Shale	3.13	1.65	0.52	0.61	1.35	1.63	0.65	27.84
S-36	Lignite	6.14	5.28	0.19	0.85	1.26	1.78	0.63	28.71

CPI: Carbon Preference Ratio

$$\text{CPI} = 2(\text{C}_{23} + \text{C}_{25} + \text{C}_{27} + \text{C}_{29}) / [\text{C}_{22} + 2(\text{C}_{24} + \text{C}_{26} + \text{C}_{28}) + \text{C}_{30}] \quad (\text{Peters and Moldwan, 1995})$$

TAR: Terrigenous/Aquatic Ratio;

$$\text{TAR} = (\text{C}_{27} + \text{C}_{29} + \text{C}_{31}) / (\text{C}_{15} + \text{C}_{17} + \text{C}_{19}) \quad (\text{Bourbonniere and Meyers, 1996})$$

P_{aq}: Proxy aqueous

$$\text{P}_{\text{aq}} = (\text{C}_{27} + \text{C}_{29} + \text{C}_{31}) / (\text{C}_{23} + \text{C}_{25} + \text{C}_{27} + \text{C}_{29} + \text{C}_{31}) \quad (\text{Ficken et al., 2000})$$

P_{wax}: Proxy wax

$$\text{P}_{\text{wax}} = (\text{C}_{23} + \text{C}_{25}) / (\text{C}_{23} + \text{C}_{25} + \text{C}_{29} + \text{C}_{31}) \quad (\text{Zheng et al., 2007})$$

ACL = Aliphatic Chain Length

$$\text{ACL} = (25\text{C}_{25} + 27\text{C}_{27} + 29\text{C}_{29} + 31\text{C}_{31} + 33\text{C}_{33}) / (\text{C}_{25} + \text{C}_{27} + \text{C}_{29} + \text{C}_{31} + \text{C}_{33}) \quad (\text{Eglinton and Hamilton, 1967})$$

Pr: Pristane; Ph: Phytane

Table 2: Terpenoid composition of the lignite and shale samples from Sonari lignite mine, western India.

Peak	compound	Base peak	Mol. ion
<i>Diterpenoids</i>			
d1	Isopimarane	163	276
d2	<i>ent</i> -beyerane	123	274
d3	possibly demethylated <i>ent</i> -beyerane?	109	260
d4	<i>ent</i> - α (H)-Kaurane	123	274
d5	18- α (H)-phyllocladane	123	274
d6	<i>ent</i> - β (H)-Kaurane	123	274
<i>Des-A-triterpenoids</i>			
1	Des-A-olean-13(18)-ene isomer?	313	328
2	Des-A-olean-13(18)-ene	313	328
3	Unknown compound	299	314
4	Des-A-olean-12-ene?	313	328
5	Des-A-lupane	123	330
6	Des-A-ursane	109	330
7	Des-A-oleanane	191	330
<i>Pentacyclic triterpenoids</i>			
8	17 α (H), 21 β (H)-25-Norhopane?	191	398
9	22,29,30-Trisnorhop-17(21)-ene	191	368
10	Unknown compound	161	408
11	Unknown compound	190	408
12	A-neo-oleana(ursa)-3(5),12-diene?	365	408
13	Unknown compound	149	396
14	30-Norneohop-13(18)-ene	191	396
15	Hop-17(21)-ene	367	410
16	Olean-12-ene+Ursa-2,12-diene	218, 218	410, 408
17	Neohop-13(18)-ene	191	410
18	$\beta\beta$ -30-Norhopane	177	398
19	$\alpha\beta$ -Homohopane(22S)	191	426
20	$\alpha\beta$ -Homohopane(22R)	191	426
21	$\beta\beta$ -Homohopane	205	426
22	$\beta\beta$ -Bishomohopane	219	440

Table 3. Results of proximate and ultimate analyses of the studied Sonari lignites.

S. No.	M	Air-dry basis (wt.%)			Dry-ash-free basis (daf) (wt.%)						Atomic ratio		Fuel Ratio (wt.%)
		Ash	S	GCV (Cal/g)	VM	FC	C	H	N	O	O/C	H/C	
S-9	4.14	17.02	2.04	4538	56.56	43.44	69.43	7.76	2.13	17.99	0.19	1.33	0.77
S-10	15.01	10.34	0.97	4542	53.53	46.47	67.11	7.57	2.68	21.11	0.24	1.34	0.87
S-11	12.37	23.82	1.19	3916	53.03	46.97	65.03	7.25	3.26	22.34	0.26	1.33	0.89
S-13	11.85	7.33	1.53	4888	45.72	54.28	68.34	6.46	2.47	20.57	0.23	1.13	1.19
S-14	12.57	17.26	1.28	4658	49.95	50.05	71.10	5.12	2.93	18.76	0.20	0.86	1.00
S-16	16.03	13.31	0.79	4380	55.19	44.81	71.70	4.33	2.90	19.75	0.21	0.72	0.81
S-17	7.04	12.34	1.94	4679	51.60	48.40	58.26	5.67	2.23	31.25	0.40	1.16	0.94
S-20	6.50	11.81	1.99	4845	51.76	48.24	61.87	6.80	2.17	26.56	0.32	1.31	0.93
S-21	15.97	11.56	0.85	4296	52.71	47.29	72.04	5.11	2.85	18.60	0.19	0.85	0.90
S-22	14.29	14.83	0.98	4365	55.67	44.33	70.07	5.96	2.82	19.54	0.21	1.01	0.80
S-23	15.54	7.08	1.10	4945	43.06	56.94	67.83	7.87	2.81	19.81	0.22	1.38	1.32
S-24	19.18	13.38	0.47	4470	53.11	46.89	70.34	6.13	3.27	19.39	0.21	1.04	0.88
S-29	16.27	10.78	0.88	4782	48.92	51.08	69.22	5.55	2.92	20.86	0.23	0.96	1.04
S-30	13.98	12.12	1.10	4708	52.34	47.66	69.63	7.24	2.72	18.69	0.20	1.24	0.91
S-35	11.43	16.56	1.39	4673	52.51	47.49	64.85	5.54	2.73	24.69	0.29	1.02	0.90
S-36	12.58	6.30	1.45	4888	45.41	54.59	64.54	5.27	2.49	25.66	0.30	0.97	1.20
S-37	13.51	8.80	1.30	4702	45.68	54.32	65.85	3.56	2.66	25.98	0.30	0.64	1.19
S-38	11.95	11.58	1.36	4543	52.84	47.16	62.84	5.26	2.51	27.37	0.33	1.00	0.89
Min.	4.14	6.30	0.47	3916	43.06	43.44	58.26	3.56	2.13	17.99	0.19	0.64	0.77
Max	19.18	23.82	2.04	4945	56.56	56.94	72.04	7.87	3.27	31.25	0.40	1.38	1.32
Avg.	12.79	12.57	1.26	4601	51.09	48.91	67.22	6.03	2.70	22.16	0.25	1.07	0.97

M= Moisture; S= Sulphur; VM= Volatile matter; FC= Fixed Carbon; GCV= Gross Calorific Value, Min= Minimum, Max.=Maximum, Wt.= Weight, Avg.= Average.

Lithology	S. No.	S ₁	S ₂	S ₃	TOC	T _{max}	HI	OI	PI	S ₂ /S ₃	GP
Shale	S-5	0.35	3.32	7.38	7.77	413	43	95	0.1	0.45	3.67
	S-12	0.04	1.07	2.68	1.99	417	54	135	0.04	0.40	1.11
	S-15	1.13	56.14	5.82	15.57	430	361	37	0.02	9.65	57.27
	S-19	0.72	5.76	13.64	17.97	405	32	76	0.11	0.42	6.48
Clay	S-26	0.06	0.61	2.19	1.17	417	52	187	0.09	0.28	0.67
	S-33	0.15	1.70	4.53	5.35	404	32	85	0.08	0.38	1.85
Avg.		0.41	11.43	6.04	8.30	414	96	103	0.07	1.93	11.84
Lignite	S-10	0.86	52.44	31.2	45.35	415	116	69	0.02	1.68	53.30
	S-14	2.53	45.96	17.07	36.95	409	124	46	0.05	2.69	48.49
	S-17	1.76	46.86	21.98	36.43	412	129	60	0.04	2.13	48.62
	S-22	1.20	20.50	24.12	31.59	405	65	76	0.06	0.85	21.70
	S-30	2.69	70.72	23.02	42.44	411	167	54	0.04	3.07	73.41
	S-36	1.16	80.62	21.65	54.84	416	147	39	0.01	3.72	81.78
Avg.		1.70	52.85	23.17	41.27	411	125	57	0.04	2.36	54.55

Table S1: Values of recorded macerals and mineral matter (in volume percentage), and the derived petrographic indices (GI, TPI, GWI & VI) of Sonari lignites

Sample No.	S-9	S-10	S-11	S-13	S-14	S-16	S-17	S-20	S-21	S-22	S-23	S-24	S-29	S-30	S-35	S-36	S-37	S-38	Min.	Max.	Avg.
Huminite (H)	40.8	49.2	63.3	44.8	37.0	68.2	69.4	48.8	74.5	69.1	39.4	81.2	55.4	55.4	50.1	54.6	37.3	34.2	34.2	81.2	54.0
Telohuminite	21.8	21.6	32.3	19.4	15.0	27.0	43.1	17.4	42.4	31.1	18.7	61.1	23.2	23.2	13.3	28.8	14.1	9.0	9.0	61.1	25.7
Textinite	0.0	0.0	0.0	0.0	0.0	0.0	0.0	0.0	0.0	0.0	0.0	0.0	0.0	1.8	0.0	0.0	0.0	0.0			
Ulminite	21.8	21.6	32.3	19.4	15.0	27.0	43.1	17.4	42.4	31.1	18.7	61.1	23.2	21.4	13.3	28.8	14.1	9.0			
Detrohuminite	16.5	25.5	29.2	23.2	21.6	39.9	24.3	29.4	32.1	36.5	19.7	18.0	31.8	29.5	35.2	24.0	23.2	23.5	16.5	39.9	26.8
Attrinite	1.7	5.7	4.5	3.4	0.9	2.1	1.5	4.5	1.3	6.6	2.4	1.7	2.6	4.5	9.0	3.6	2.0	3.4			
Densinite	14.8	19.8	24.7	19.8	20.7	37.8	22.8	24.9	30.8	29.9	17.3	16.3	29.2	25.0	26.2	20.4	21.2	20.1			
Gelohuminite	2.5	2.1	1.8	2.2	0.4	1.3	2.0	2.0	0.0	1.5	1.0	2.1	0.4	2.7	1.6	1.8	0.0	1.7	0.0	2.7	1.5
Corpohuminite	2.5	2.1	1.8	2.2	0.4	1.3	2.0	2.0	0.0	1.5	1.0	2.1	0.4	2.7	1.6	1.8	0.0	1.7			
Liptinite (L)	4.6	20.1	17.3	14.5	7.5	8.5	7.0	13.5	4.4	11.6	19.7	5.9	5.5	11.2	9.3	8.7	3.0	12.3	3.0	20.1	10.3
Sporinite	0.4	4.9	2.2	3.0	0.9	2.6	2.0	3.0	2.2	3.0	6.2	1.3	2.1	2.7	1.6	2.9	0.5	2.1			
Cutinite	1.3	5.3	4.0	3.7	1.3	2.1	2.0	3.5	0.9	0.0	6.6	0.4	0.4	2.2	1.6	1.8	0.5	1.7			
Suberinite	0.0	1.1	1.3	2.2	0.0	0.0	0.0	0.0	0.0	0.0	0.0	0.0	0.0	0.0	0.0	0.0	0.0	0.0			
Resinite	2.1	4.6	6.7	2.2	4.0	2.1	2.0	2.5	0.4	7.6	3.8	2.9	2.1	3.6	3.5	2.9	2.0	4.7			
Liptodetrinite	0.8	4.2	3.1	3.4	1.3	1.7	1.0	4.5	0.9	1.0	3.1	1.3	0.9	2.7	2.6	1.1	0.0	3.8			
Inertinite (I)	27.1	20.5	5.0	31.0	39.2	12.1	9.9	23.7	13.9	6.2	36.4	7.5	31.8	17.8	26.6	27.9	33.4	32.2	5.0	39.2	22.3
Semifusinite	9.3	8.8	1.8	14.2	17.2	2.6	3.0	8.1	6.7	1.0	22.8	1.3	20.2	6.3	16.3	15.7	14.6	15.4			
Fusinite	0.4	0.0	0.0	0.0	4.8	0.0	0.0	4.0	0.0	0.0	0.0	0.0	0.0	2.5	1.0	3.6	0.0	0.0			
Funginite	3.4	3.5	3.2	9.0	7.0	6.0	5.1	5.6	4.5	5.2	2.4	6.2	3.0	4.5	2.7	2.9	5.6	3.8			
Inertodetrinite	14.0	8.2	0.0	7.8	10.2	3.5	1.8	6.0	2.7	0.0	11.2	0.0	8.6	4.5	6.6	5.7	13.2	13.0			
Mineral Matter (TOTAL)	27.5	10.2	14.4	9.7	16.3	11.2	13.7	14.0	7.2	13.1	4.5	5.4	7.3	15.6	14.0	8.8	26.3	21.3	4.5	27.5	13.4
Others	16.9	8.1	9.9	6.3	5.3	8.2	8.1	9.0	6.3	10.1	4.5	5.4	3.4	10.7	10.9	6.2	9.6	13.2			
Pyrite	10.6	2.1	4.5	3.4	11.0	3.0	5.6	5.0	0.9	3.0	0.0	0.0	3.9	4.9	3.1	2.6	16.7	8.1			
Fluorescing (H)	8.7	14.5	22.9	11.6	15.4	15.9	18.2	14.4	18.3	22.9	8.6	6.7	16.3	10.3	17.6	12.0	9.6	12.4			
Non-fluorescing (H)	32.1	34.7	40.4	33.2	21.6	52.3	51.2	34.4	56.2	46.2	30.8	74.5	39.1	45.1	32.5	42.6	27.7	21.8			

Total Fluorescing (H+L)	13.3	34.6	40.2	26.1	22.9	24.4	25.2	27.9	22.7	34.5	28.3	12.6	21.8	21.5	26.9	20.7	12.6	24.7			
Non-fluorescing (H+I+M)	86.7	65.4	59.8	73.9	77.1	75.6	74.8	72.1	77.3	65.5	71.7	87.4	78.2	78.5	73.1	79.3	87.4	75.3			
H (mmf)	56.3	54.8	73.9	49.6	44.2	76.8	80.4	56.7	80.3	79.5	41.3	85.8	59.8	65.6	58.3	59.9	50.6	43.5	41.3	85.8	62.1
L (mmf)	6.3	22.4	20.2	16.1	9.0	9.6	8.1	15.7	4.7	13.3	20.6	6.2	5.9	13.3	10.8	9.5	4.1	15.6	4.1	22.4	11.8
I (mmf)	37.4	22.8	5.8	34.3	46.8	13.6	11.5	27.6	15.0	7.1	38.1	7.9	34.3	21.1	30.9	30.6	45.3	40.9	5.8	46.8	26.2
GI	1.36	1.66	6.19	1.20	0.90	4.65	5.96	1.57	4.82	4.88	0.95	8.64	1.53	2.04	1.15	1.62	1.00	0.87	0.87	8.64	2.83
TPI	0.81	0.70	1.17	0.70	0.64	0.65	1.73	0.66	1.22	0.89	0.64	3.51	0.58	0.84	0.38	1.15	0.39	0.29	0.29	3.51	0.94
GWI	1.10	0.99	1.04	1.13	1.87	1.57	0.69	1.50	0.84	1.03	1.04	0.40	1.36	1.22	1.62	0.78	1.59	2.23	0.40	2.23	1.22
VI	1.13	1.22	1.50	1.30	1.31	0.81	1.92	0.96	1.47	1.14	1.71	3.47	1.16	1.10	0.84	1.81	0.87	0.82	0.81	3.47	1.36
GI (Gelification Index) = (Ulminite+Densinite+Corpohuminite+Gelinite)/(Textinite+Attrinite+Inertinite)																			(Kalaitzidis et al., 2004)		
TPI (Tissue Preservation Index) = (Textinite+Ulminite+Corpohuminite+Fusinite)/(Attrinite+Densinite+Gelinite+Inertodetrinite)																			(Kalaitzidis et al., 2004)		
GWI (Groundwater Index) = (Densinite+Corpohuminite+Gelinite+(Ash/2))/(Textinite+Ulminite+Attrinite)																			(Kalaitzidis et al., 2004) and (Stock et al., 2016)		
VI (Vegetation Index) = (Textinite +Ulminite +Suberinite +Resinite+ Fusinite+Semifusinite)/(Attrinite+Densinite +Sporinite+Cutinite+ Alginite+Bituminite+Liptodetrinite+Inertodetrinite)																			(Kalaitzidis et al., 2004)		

Table S2. Result of palynofacies analysis of the studied Sonari samples (classification based on Mendonça Filho et al., 2012). PPI and TAI calculations are according to Mendonça Filho et al., 2010 and Staplin, 1969, 1977, respectively)

S. no.	Phytolasts (%)					Total	AOM (%)		Total	Palynomorphs (%)		Total	PPI	TAI	PF-Zone
	O	N-O					AOM	R		Te	Ma				
		Cu	NB	B	Fu										
S-1	4.05	3.38	57.43	9.80	0.00	74.66	17.91	0.00	17.91	7.43	0.00	7.43	0.46	2.00+	I
S-2	14.75	5.04	57.91	3.60	0.72	82.01	15.47	0.72	16.19	1.80	0.00	1.80	0.79	2.00	I
S-3	16.95	1.72	58.62	1.72	0.57	79.60	19.25	0.00	19.25	1.15	0.00	1.15	0.91	2.00	I
S-4	18.18	7.62	37.24	8.80	0.88	72.73	24.63	0.29	24.93	2.35	0.00	2.35	1.26	2.00+	I
S-5	14.37	5.17	48.56	4.02	1.15	73.28	21.55	0.29	21.84	3.16	1.72	4.89	0.85	2.00	I
S-6	28.42	7.24	41.02	4.29	0.54	81.50	15.01	0.54	15.55	2.41	0.54	2.95	1.71	2.25	I
S-7	6.86	5.23	58.50	6.54	1.96	79.08	13.73	0.00	13.73	5.23	1.96	7.19	0.53	2.00	I
S-8	14.24	2.53	65.19	2.22	0.63	84.81	12.66	0.00	12.66	2.53	0.00	2.53	0.74	2.00	I
S-9	21.32	0.98	49.51	2.94	0.98	75.74	22.30	0.00	22.30	1.96	0.00	1.96	1.35	2.00+	I
S-10	37.98	1.19	44.21	1.78	0.30	85.46	13.35	0.00	13.35	1.19	0.00	1.19	2.48	2.00+	I
S-11	11.47	2.51	22.58	1.79	0.72	39.07	57.35	1.08	58.42	2.51	0.00	2.51	1.36	2.00	II
S-12	4.52	3.87	54.52	9.35	2.90	75.16	10.65	1.29	11.94	10.65	2.26	12.90	0.47	2.00	I
S-13	70.32	0.97	16.13	0.97	0.32	88.71	11.29	0.00	11.29	0.00	0.00	0.00	6.77	2.60	I
S-14	65.57	4.45	9.37	3.04	0.94	83.37	16.63	0.00	16.63	0.00	0.00	0.00	6.79	2.50	I
S-15	7.21	0.90	47.15	0.90	0.60	56.76	43.24	0.00	43.24	0.00	0.00	0.00	0.62	2.25	III
S-16	17.18	1.18	49.41	0.94	0.47	69.18	29.18	0.00	29.18	1.65	0.00	1.65	1.05	2.00	I
S-17	53.66	2.20	31.46	0.73	0.24	88.29	10.49	0.00	10.49	1.22	0.00	1.22	4.03	2.50	I
S-18	11.54	3.08	60.00	4.23	0.77	79.62	18.08	0.00	18.08	2.31	0.00	2.31	0.68	2.00	I
S-19	39.33	2.25	43.54	1.69	0.56	87.36	11.24	0.00	11.24	1.40	0.00	1.40	2.61	2.00	I
S-20	61.73	1.23	24.69	1.65	0.00	89.30	9.47	0.00	9.47	1.23	0.00	1.23	5.09	2.00+	I
S-21	33.44	1.67	41.14	2.01	1.34	79.60	17.39	0.00	17.39	3.01	0.00	3.01	2.26	2.00+	I
S-22	12.66	2.18	60.26	2.18	0.44	77.73	20.52	0.00	20.52	1.75	0.00	1.75	0.73	2.00	I
S-23	48.24	1.26	30.65	1.01	0.50	81.66	15.33	0.00	15.33	3.02	0.00	3.02	4.06	2.25+	I
S-24	23.75	1.88	51.88	1.25	0.63	79.38	19.38	0.00	19.38	1.25	0.00	1.25	1.36	2.00	I
S-25	21.52	3.94	43.03	3.94	1.52	73.94	16.67	1.52	18.18	6.06	1.82	7.88	1.39	2.00	I
S-26	12.20	0.70	13.59	1.39	0.00	27.87	68.99	0.00	68.99	1.39	1.74	3.14	2.49	2.00+	II
S-27	9.33	2.93	56.53	1.87	0.53	71.20	26.13	0.00	26.13	1.60	1.07	2.67	0.62	2.00	I
S-28	14.69	3.85	60.84	5.94	1.40	86.71	10.49	0.00	10.49	2.80	0.00	2.80	0.78	2.00+	I
S-29	36.15	1.17	46.65	1.17	0.58	85.71	14.29	0.00	14.29	0.00	0.00	0.00	2.30	2.00	I
S-30	39.05	2.11	41.95	2.37	0.53	86.02	12.40	0.00	12.40	1.58	0.00	1.58	2.62	2.00+	I
S-31	19.59	7.89	52.92	2.63	0.00	83.04	14.04	0.00	14.04	2.92	0.00	2.92	0.98	2.00	I
S-32	32.58	2.27	48.23	1.77	0.51	85.35	13.13	0.00	13.13	1.52	0.00	1.52	1.88	2.00	I
S-33	9.16	1.62	45.01	3.23	1.62	60.65	39.35	0.00	39.35	0.00	0.00	0.00	0.72	2.00+	III
S-34	11.81	6.27	60.15	5.17	0.74	84.13	15.87	0.00	15.87	0.00	0.00	0.00	0.64	2.00	I
S-35	40.27	12.88	32.05	3.29	0.82	89.32	10.68	0.00	10.68	0.00	0.00	0.00	2.55	2.00+	I
S-36	70.56	16.75	5.08	2.03	0.00	94.42	5.58	0.00	5.58	0.00	0.00	0.00	5.56	2.60	I

S-37	53.25	2.11	35.26	1.05	1.05	92.72	4.21	0.00	7.28	0.00	0.00	0.00	4.15	2.50	I
S-38	88.14	0.85	3.39	1.69	0.85	94.92	5.08	0.00	5.08	0.00	0.00	0.00	9.03	2.70	I
Min.	4.05	0.70	3.39	0.73	0.00	27.87	4.21	0.00	5.08	0.00	0.00	0.00	0.46	2.00	
Max.	88.14	16.75	65.19	9.80	2.90	94.92	68.99	1.52	68.99	10.65	2.26	12.90	9.03	2.70	
Avg.	28.84	3.55	42.25	3.03	0.74	78.42	19.03	0.15	19.26	2.03	0.29	2.32	2.23	2.15	

O= Opaque; N-O= Non-opaque; Cu= Cuticle; NB= Non-Biostructure; B= Biostructure; Fu= Fungal; AOM= Amorphous Organic Matter; R= Resin; Te=Terrestrial; Ma= Marine; PPI: Phytoclast Preservation Index; TAI: Thermal Alteration Index; PF= Palynofacies; Min.= Minimum; Max.= Maximum; Avg.= Average

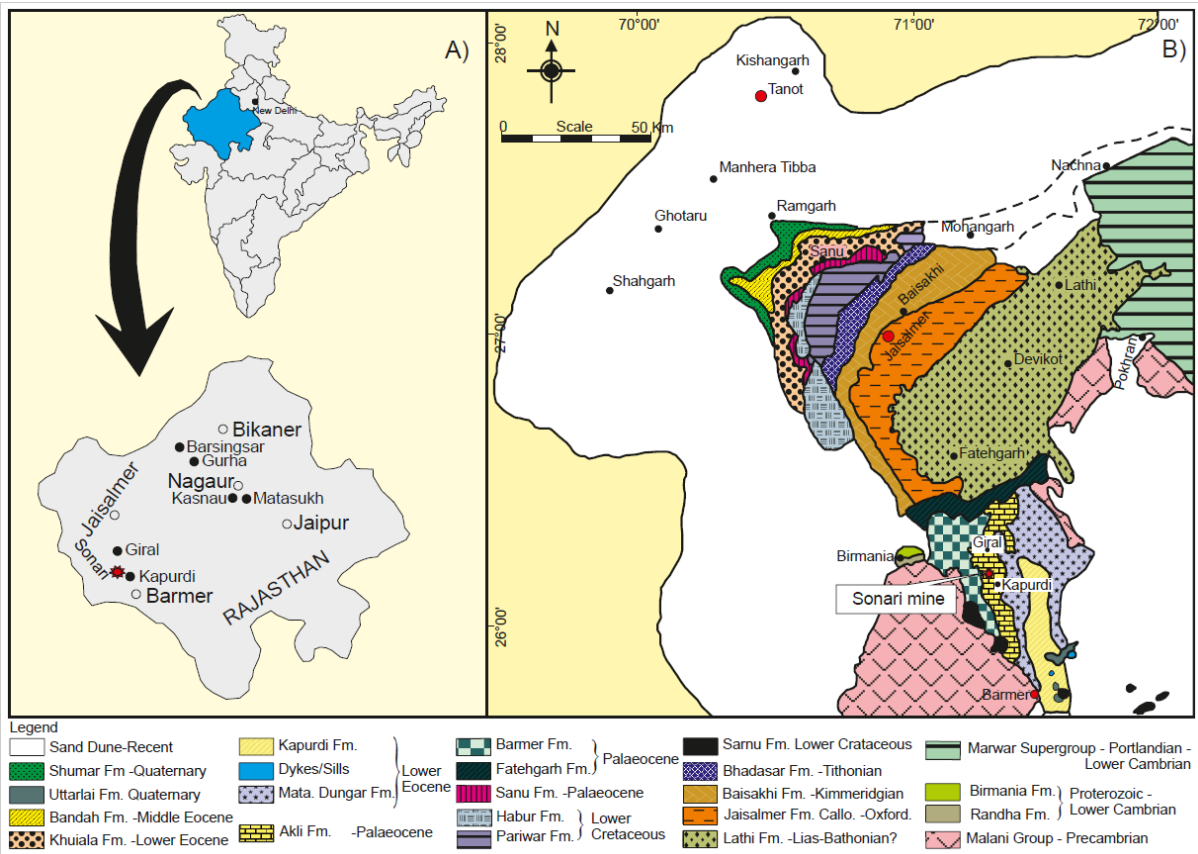


Fig. 1. Geographical position (a) and different geological formations (b) of Barmer Basin (Rajasthan), north-western India (modified after Rai et al., 2013).

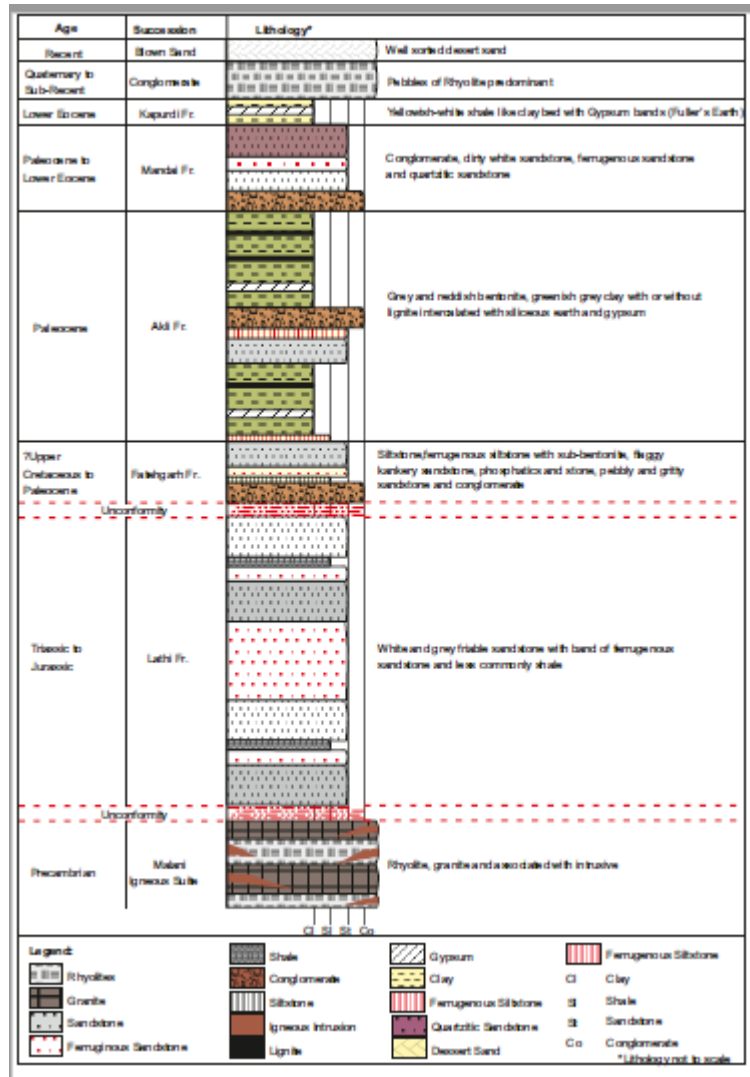


Fig. 2. General stratigraphic column of Barmer Basin, north-western India.

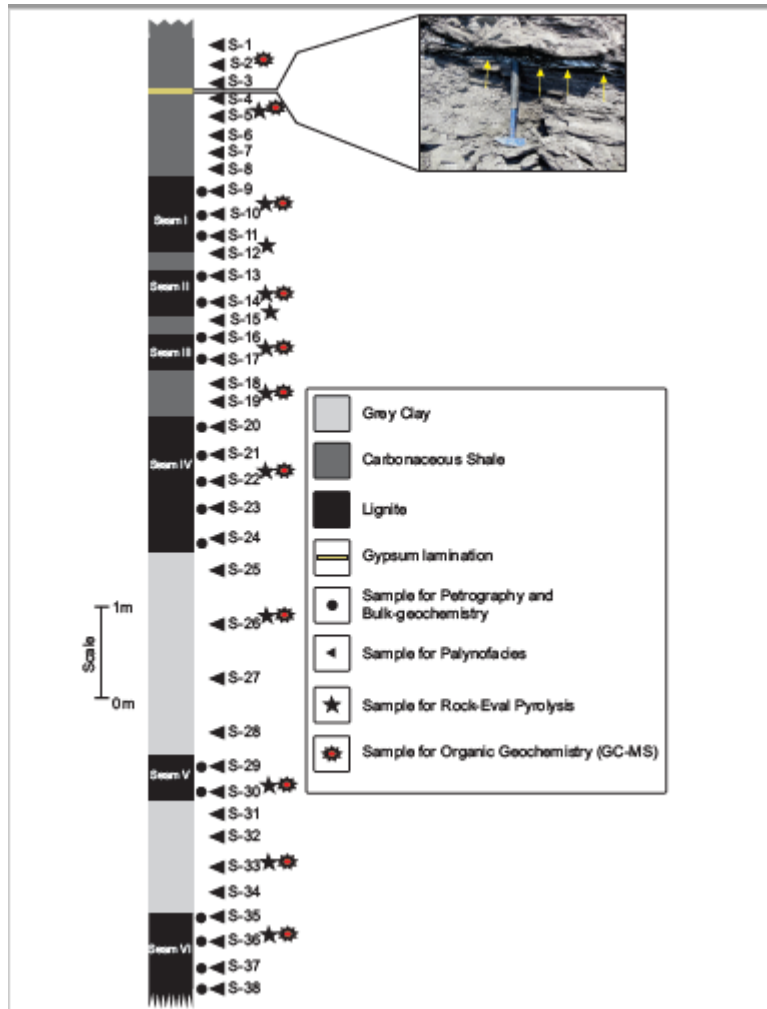


Fig. 3. Litho-column of Sonari mine displaying the different lithological units and the sample positions.

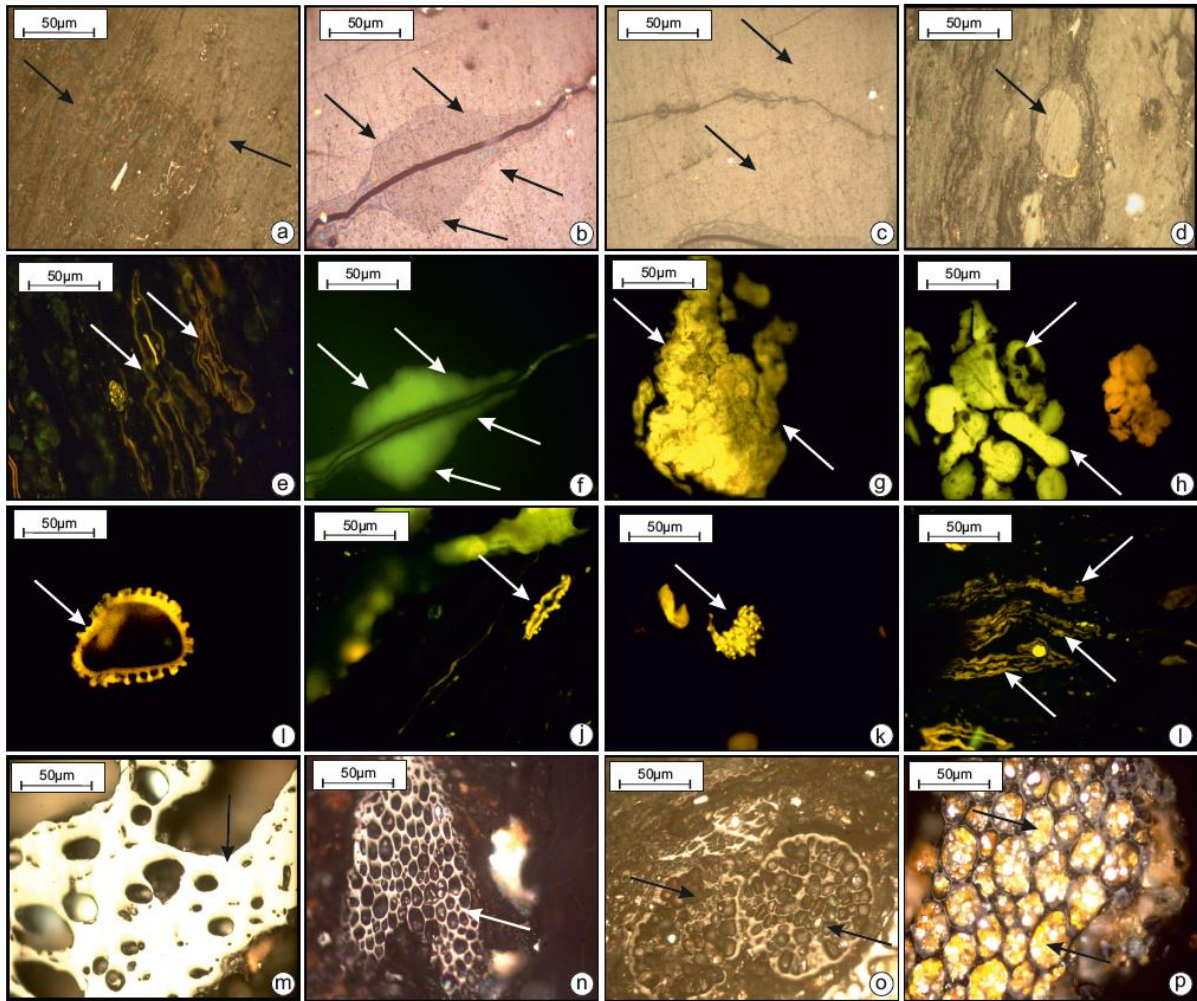


Fig. 4. Photomicrographs representing the various macerals and maceral-mineral associations of the Sonari lignite: a-c) ulminite, d) corpohuminite (arrow), e) cutinite, f) exsudatinite/oil smear (fluorescence view of b), g-h) resinite, i-k) sporinite, l) cluster of sporinite, m) fusinite, n) semifusinite, o) funginite, p) pyrite fillings. Photomicrographs were taken under reflected white light (a–d and m–p) and in fluorescence mode (e–l).

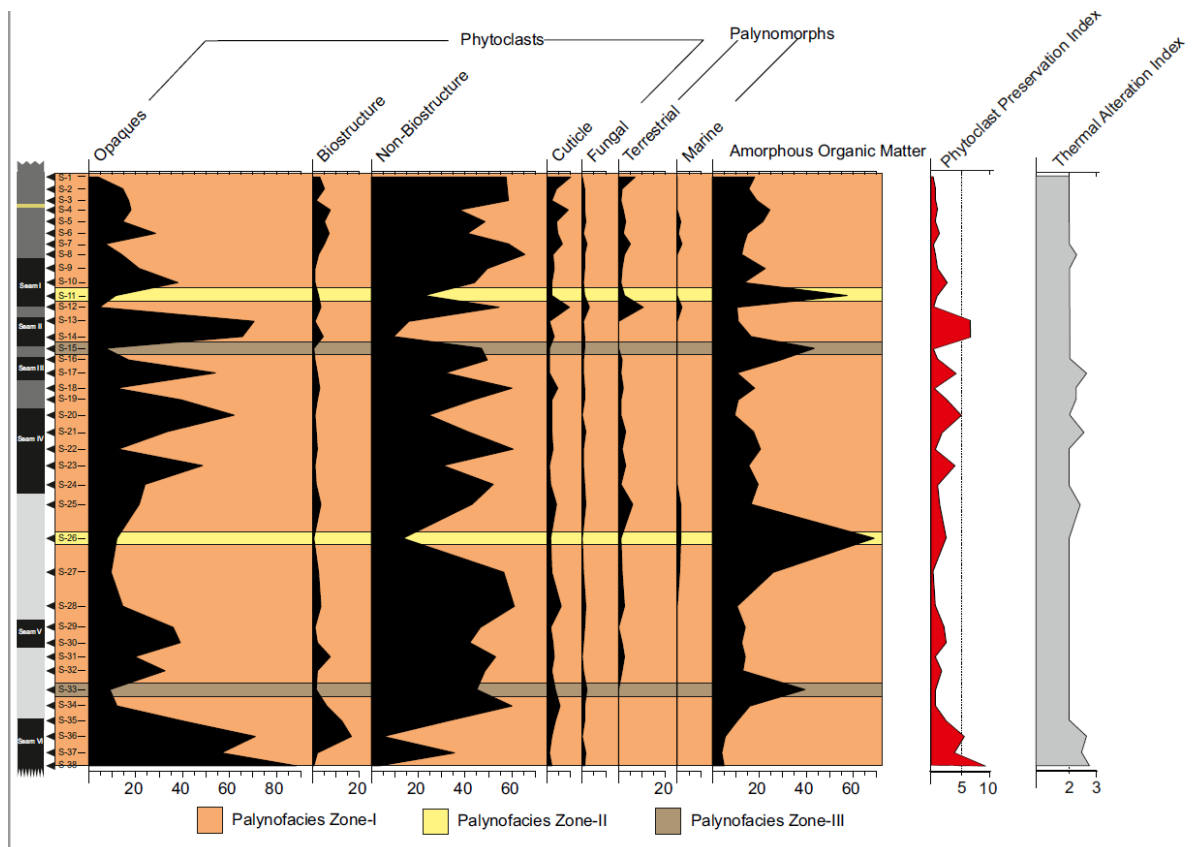


Fig. 5. Frequency pattern of dispersed organic matter (kerogen) and the facies recognized in the studied Sonari sediments and the plotting of Phytoclast Preservation Index (PPI) and Thermal Alteration Index (TAI).

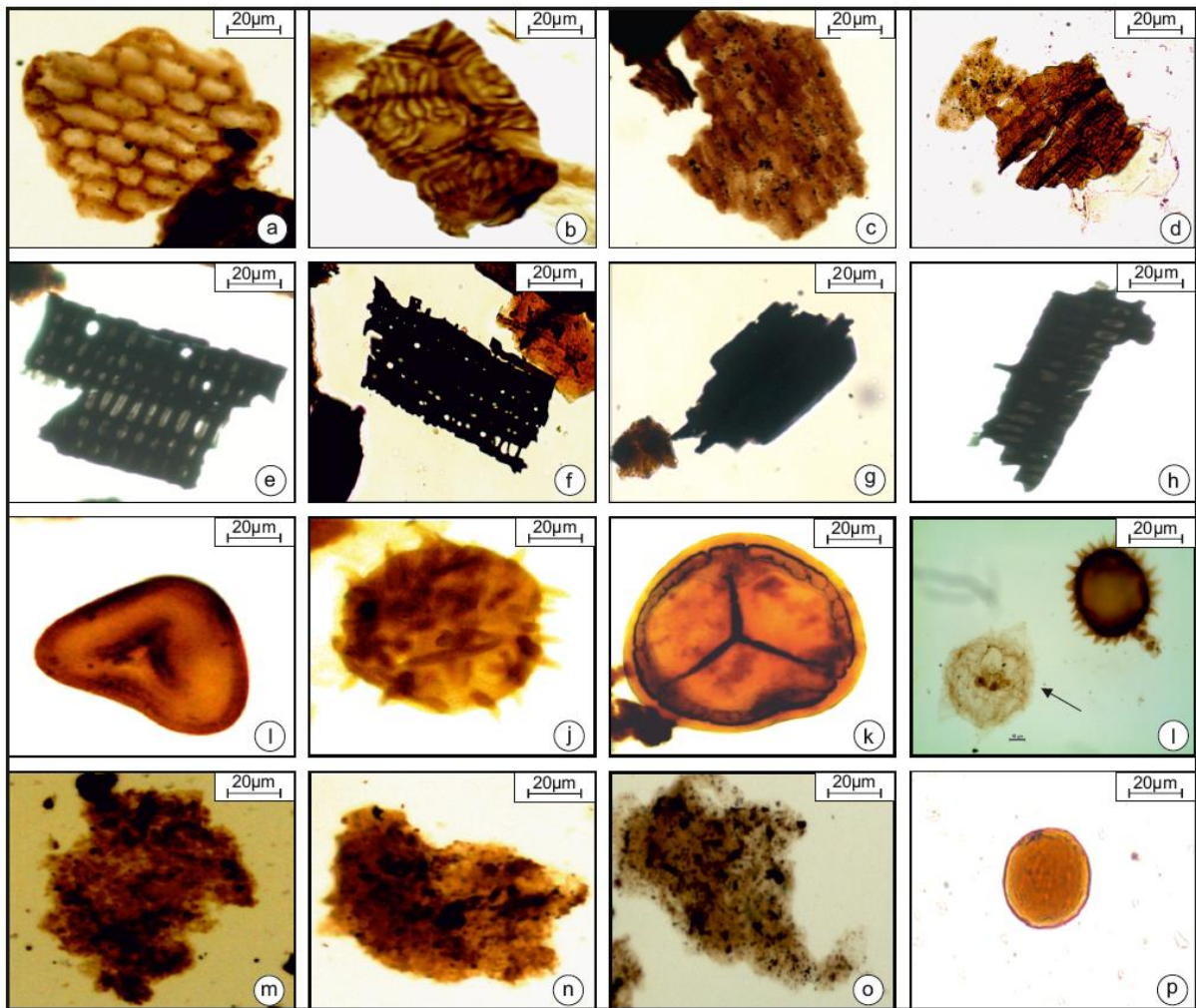


Fig. 6. Photomicrographs illustrating various components of dispersed organic matter (kerogen): a-b) cuticle, c-d) biostructure phytoclasts, e-h) opaque phytoclasts, i-k) palynomorphs, l) dinoflagellate cyst (arrow), m-o) AOM, p) resin.

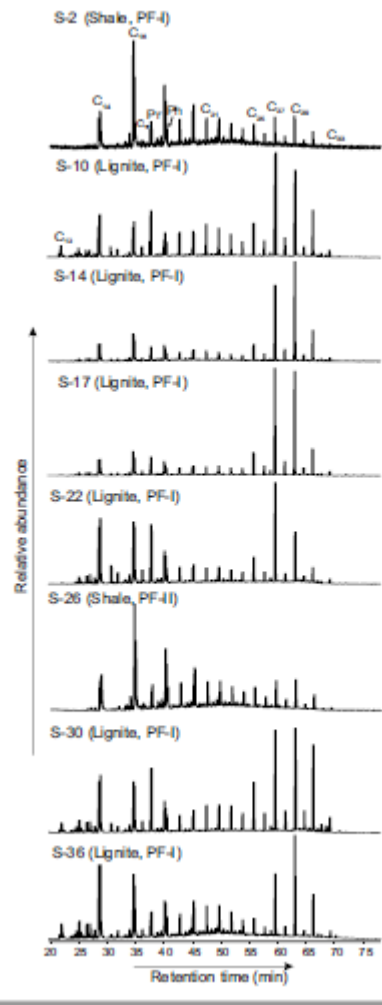


Fig. 7. The distribution of *n*-alkane (SIM *m/z* 57) of Sonari samples. Digits denoting the carbon number in the *n*-alkane chain.

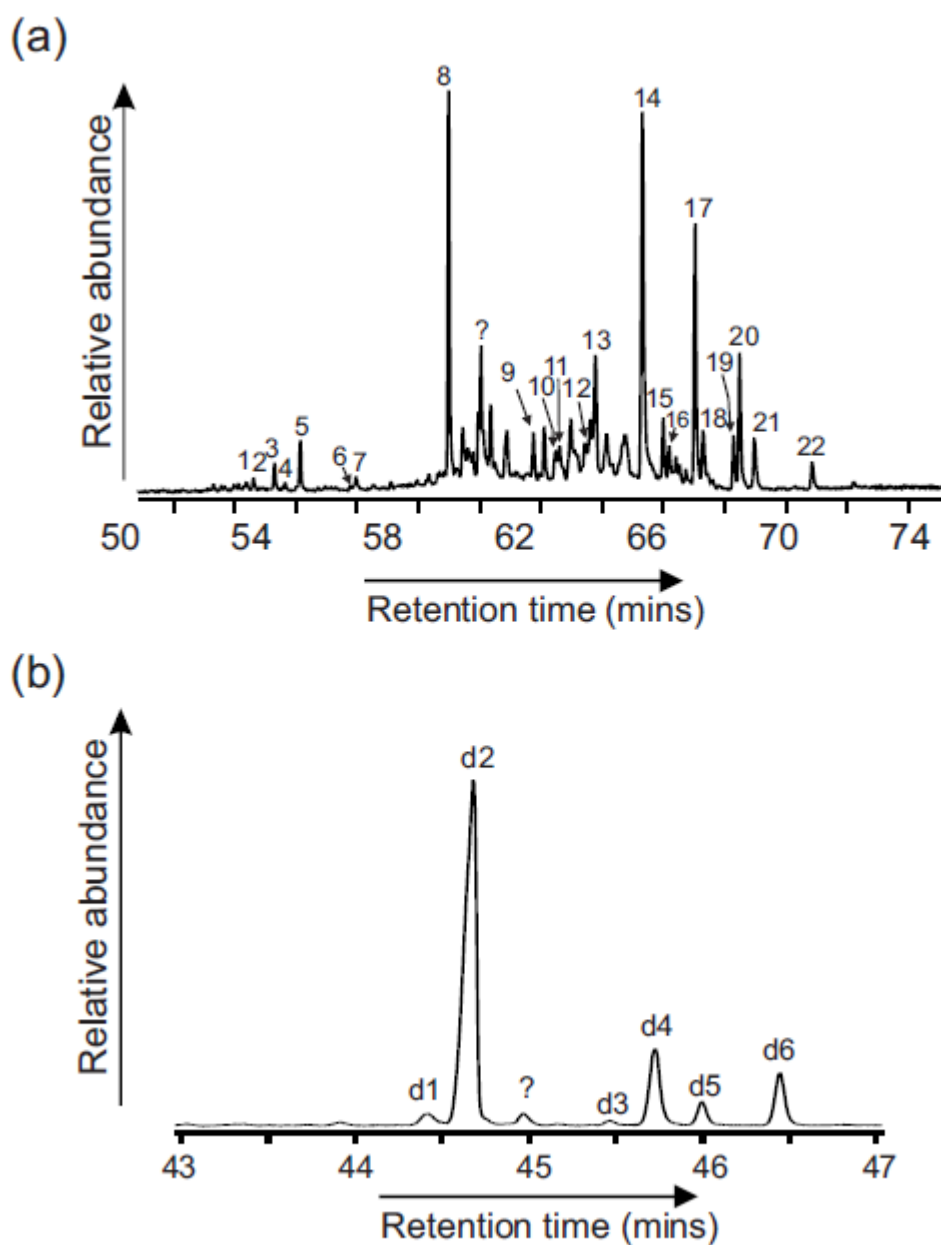


Fig. 8. Triterpenoid (a) and diterpenoid (b) distribution in the Sonari samples. The numbers correspond to the compounds listed in Table 2.

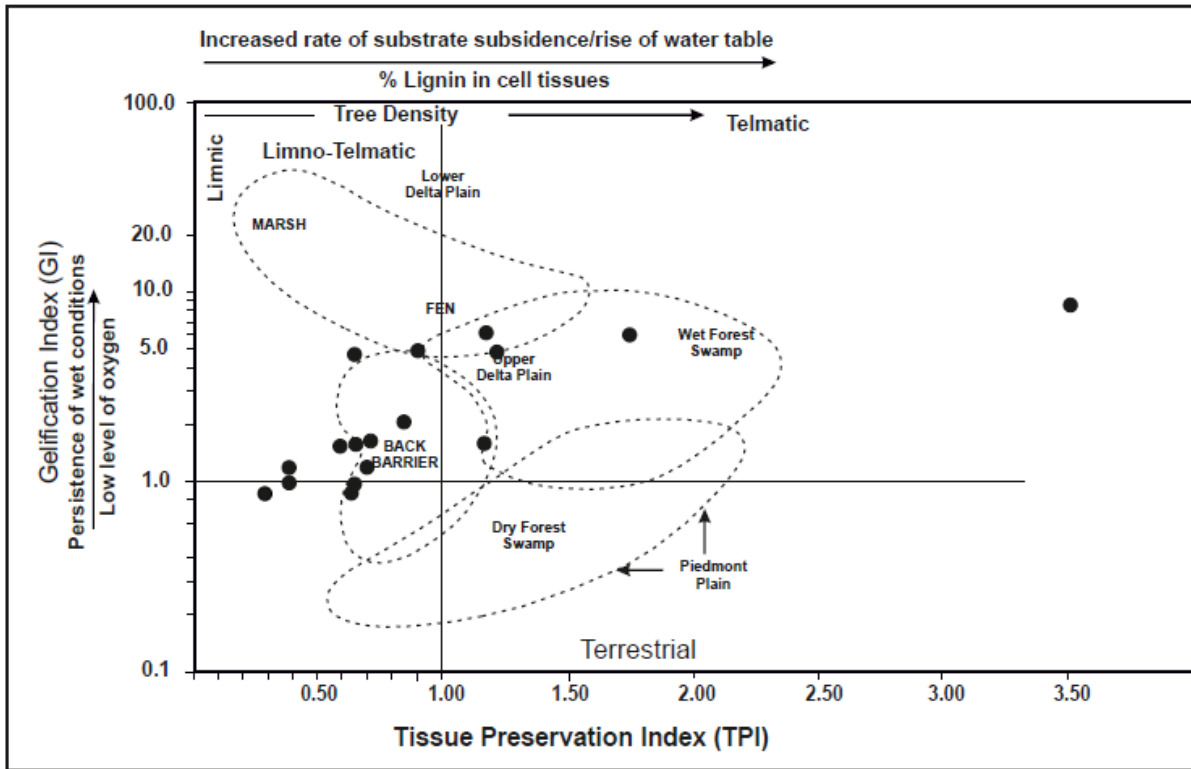


Fig. 9. GI-TPI indices showing the general trend of peat-swamp evolution (after Diessel, 1992).

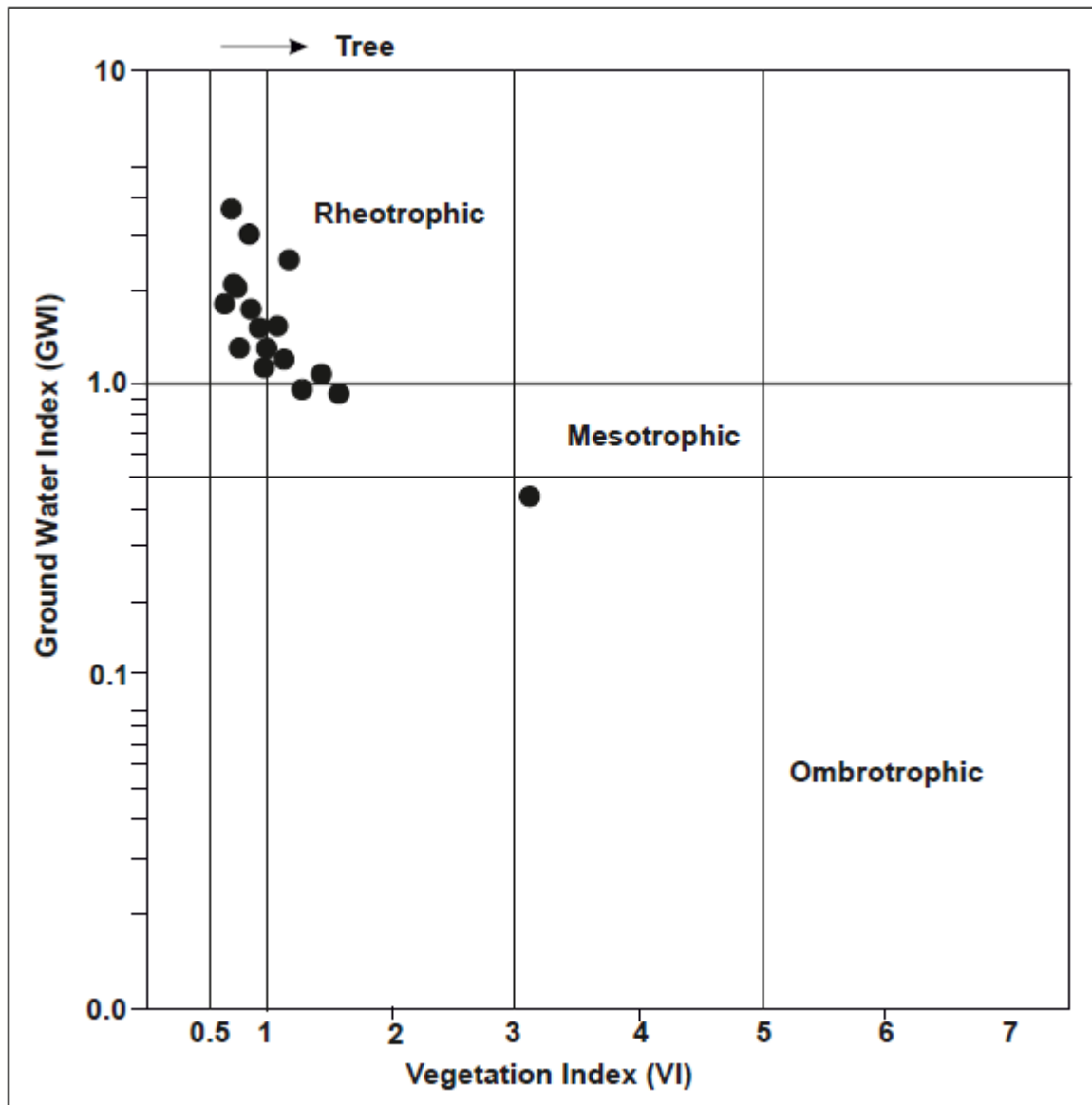


Fig. 10. VI-GWI indices representing the trend of groundwater level and vegetation type during peat accumulation (after Calder et al., 1991).

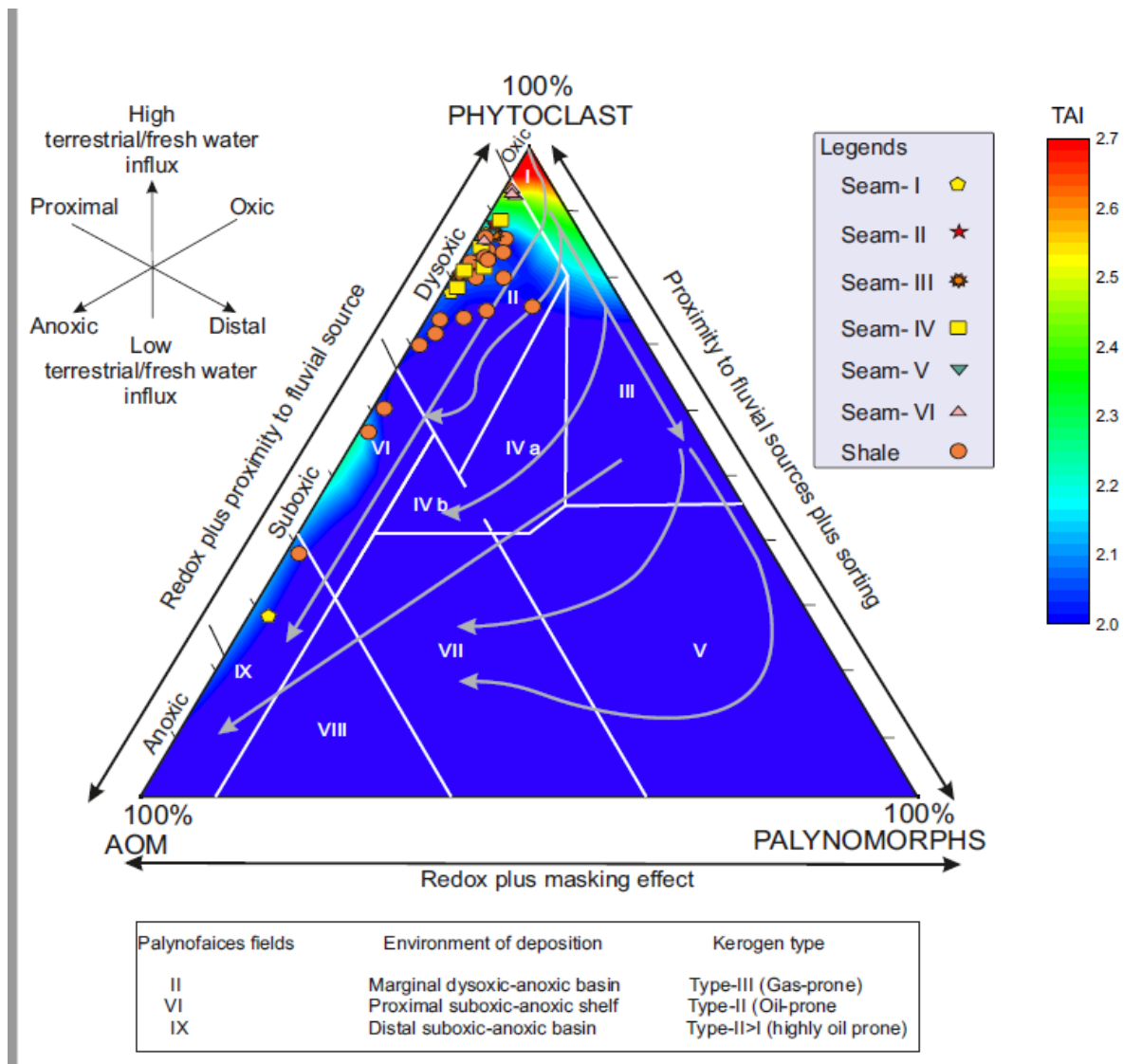


Fig. 11. Tyson's APP diagram integrated with thermal alteration index (TAI; coloured background) indicating the depositional fields, their corresponding maturation level and type of kerogen for the Sonari succession.

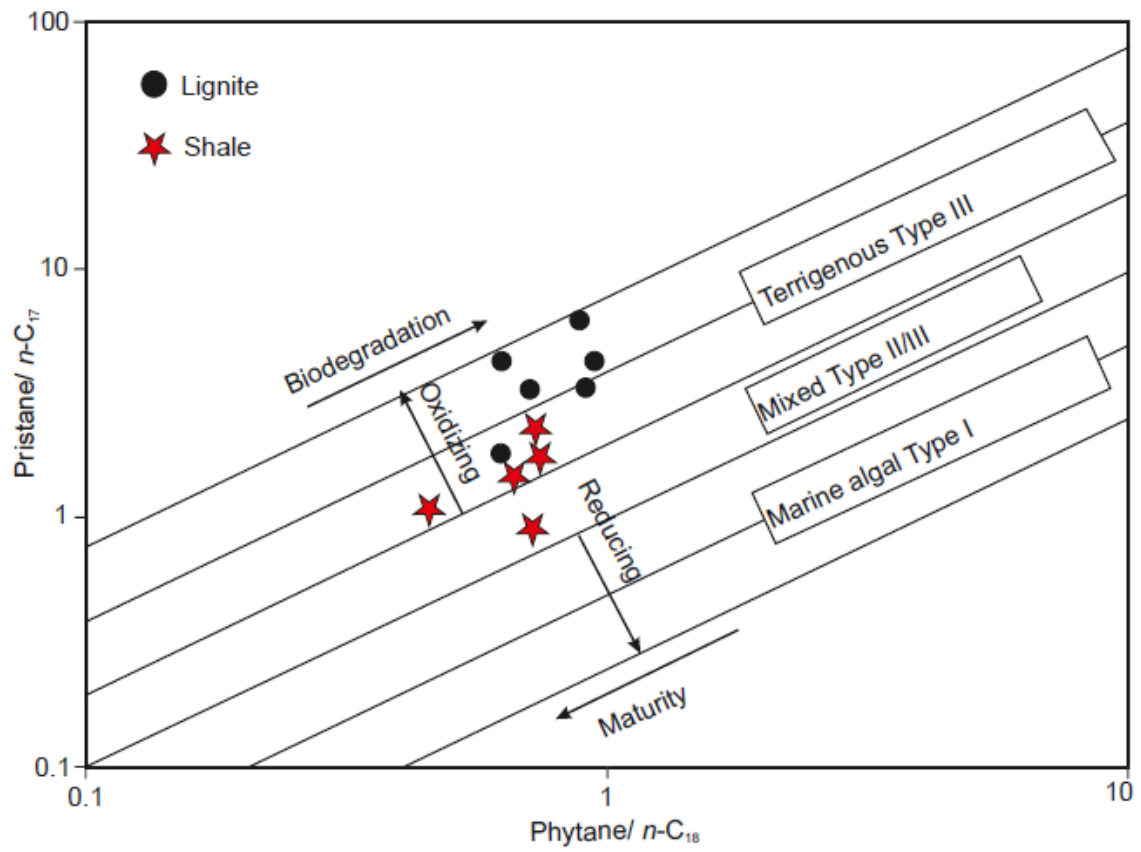


Fig. 12. The plotting of Pristane/*n*-C₁₇ vs. phytane/*n*-C₁₈ of the studied samples.

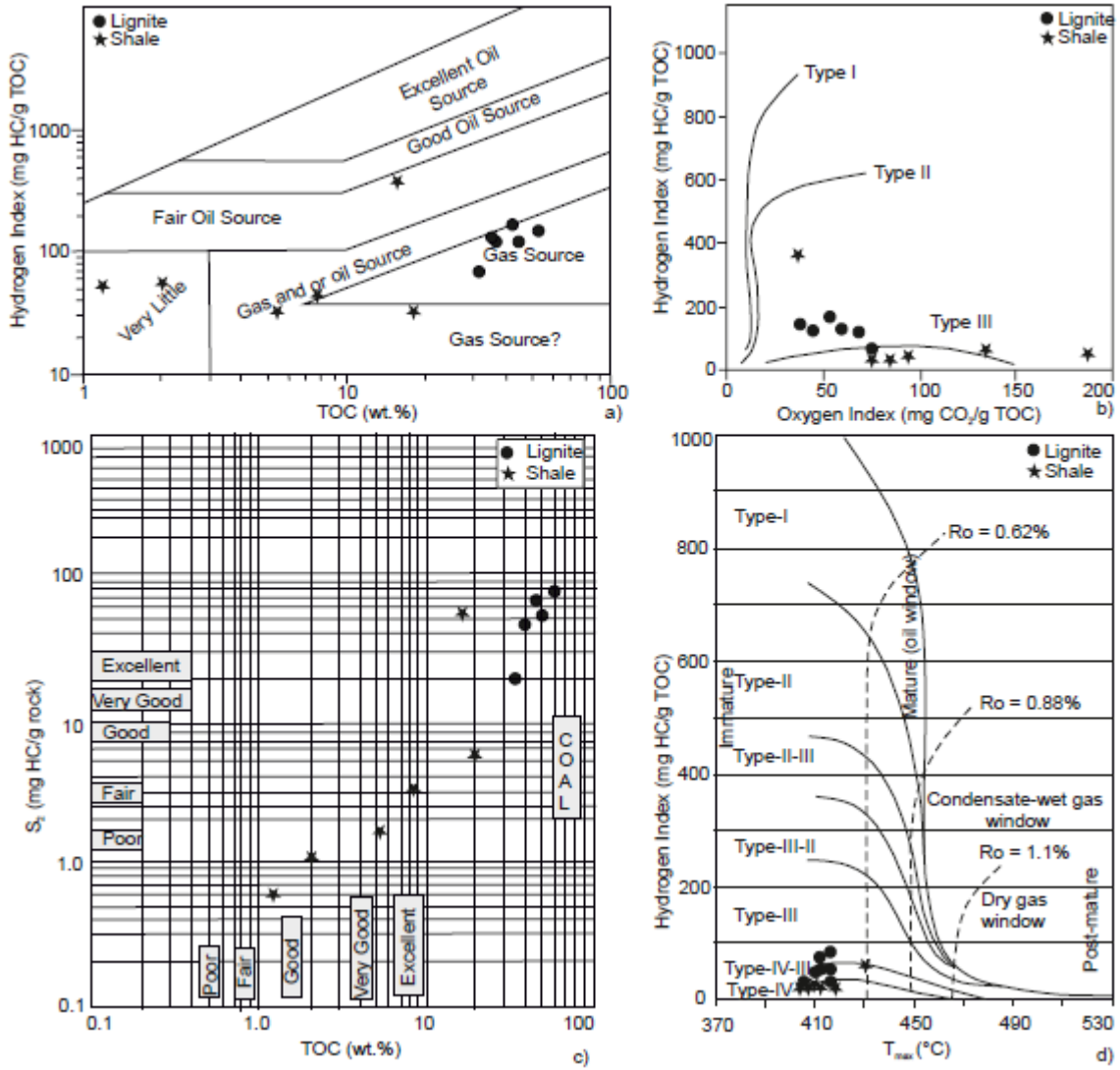


Fig. 13. The cross plots indicating relationship between: a) Hydrogen Index vs. Total Organic Carbon, b) Hydrogen Index vs. Oxygen Index, c) S₂ vs. Total Organic Carbon, d) HI vs. T_{max}.

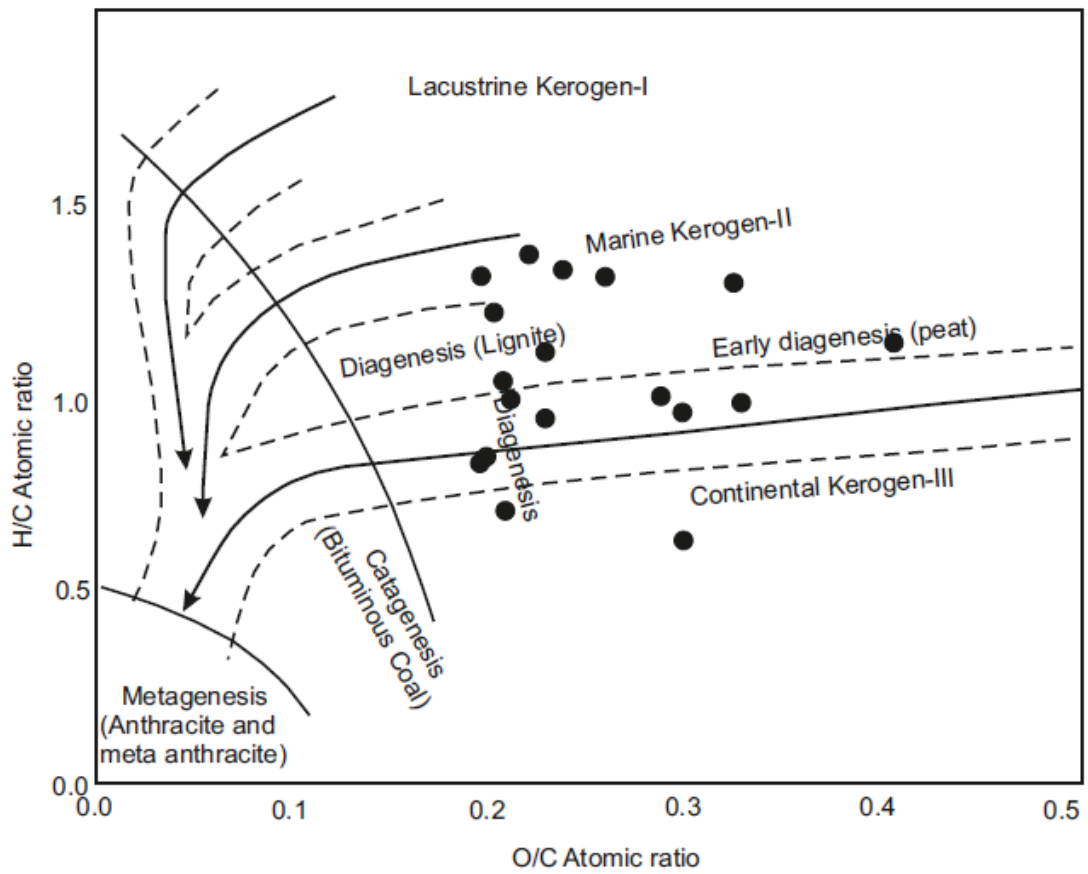


Fig. 14. The plotting H/C vs. O/C ratios (atomic) on pseudo-Van Krevelen plot of the Sonari samples.